

1 **Enhanced Sulfate Formation in Mixed Biomass Burning and Sea-salt**
2 **Particles-Interactions Mediated by Photosensitization: Effects of**
3 **Chloride, and Nitrogen-containing Compounds and Atmospheric**
4 **Aging**

5 Rongzhi Tang^{1,2}, Jialiang Ma³, Ruifeng Zhang⁴, Weizhen Cui¹, Yuanyuan Qin⁵, Yangxi Chu⁶,
6 Yiming Qin¹, Alexander L. Vogel³, Chak K. Chan^{4,*}

7 ¹ School of Energy and Environment, City University of Hong Kong, Hong Kong, China

8 ² Shenzhen Research Institute, City University of Hong Kong, Shenzhen 518057, China

9 ³ Institute for Atmospheric and Environmental Sciences, Goethe-University Frankfurt, 60438
10 Frankfurt am Main, Germany

11 ⁴ Division of Physical Science and Engineering, King Abdullah University of Science and
12 Technology (KAUST), Thuwal 23955-6900, Kingdom of Saudi Arabia

13 ⁵ College of Resources and Environment, University of Chinese Academy of Sciences, Beijing,
14 100049, China

15 ⁶ State Key Laboratory of Environmental Criteria and Risk Assessment, Chinese Research
16 Academy of Environmental Sciences, Beijing, 100012, China

17 *Correspondence to:* Chak K. Chan (chak.chan@kaust.edu.sa)

18 **Abstract**

19 Discrepancies persist between modeled simulations and measured sulfate concentrations in
20 marine boundary layer, especially when the marine air was influenced by biomass burning
21 plume. However, there is a notable dearth of research conducted on the interactions between
22 sea-salt aerosol and biomass burning plume, impeding a comprehensive understanding of the
23 sulfate formation. Recent research has suggested that photosensitized oxidation can be an
24 effective pathway for the oxidation of SO₂ based on a limited number of model photosensitizers.
25 ~~However, there is a notable dearth of research conducted on complex chemical systems,~~
26 ~~impeding a comprehensive understanding of sulfate formation in photosensitization.~~ This work
27 studied sulfate formation by mixing real biomass burning (BB) extracts and NaCl, mimicking
28 internal mixtures of BB and sea-salt particles. Significant enhancement of sulfate formation
29 was observed for BB-NaCl particles compared to incense burning (IS)-NaCl particles. For fresh
30 particles, the sulfate formation rate followed the trend of corn straw (CS)-NaCl>rice straw
31 (RS)-NaCl>wheat straw (WS)-NaCl>IS-NaCl. The filter aging Aged particles was were
32 produced achieved by exposing them to OH[•] through irradiating the filters directly with UV
33 irradiation lights. Aged particles showed changes in sulfate formation rates, with the highest
34 enhancement by RS-NaCl due to interactions between RS and NaCl. Model experiments spiked

35 with nitrogen-containing organic compounds (NOCs), such as pyrazine (CHN) and 4-
36 nitrocatechol (CHON), revealed positive effects of chloride in the PS-CHON system and
37 negative effects in the PS-CHN system. Our work suggests that BB reaching or near coastal
38 areas could affect sulfate formation via photosensitizer-mediated reactions, potentially
39 exacerbating air quality concerns.

40 **Keywords:** sulfate formation, biomass burning, photosensitization, sea-salt aerosol, chloride

41 1 Introduction

42 ~~Sulfate is a critical constituent of atmospheric particulate matter, exerting substantial influence~~
43 ~~on atmospheric radiative forcing, air quality, and human health (Fuzzi et al., 2015; Nel, 2005;~~
44 ~~Charlson et al., 1992). The commonly recognized sulfate formation mechanisms include gas-~~
45 ~~phase SO₂ oxidation by OH radicals (Stockwell and Calvert, 1983) and stabilized Criegee~~
46 ~~intermediates (sCIs) (Mauldin Iii et al., 2012) and multiphase and heterogeneous SO₂ oxidation~~
47 ~~by H₂O₂, O₃, NO₂, organic peroxides and O₂-catalyzed transition metal ions (TMI) (Seinfeld~~
48 ~~and Pandis, 2016; Wang et al., 2020a; Liu and Abbatt, 2021; Liu et al., 2020; Wang et al., 2021b).~~
49 ~~More recently, some new sulfate formation pathways, e.g., in particle nitrate photolysis (Gen~~
50 ~~et al., 2019a, b), triplet SO₂ chemistry (Donaldson et al., 2016; Gong et al., 2022), SO₂ oxidation~~
51 ~~on acidic microdroplets (Hung and Hoffmann, 2015), photosensitizer mediated SO₂ oxidation~~
52 ~~(Tang et al., 2023; Wang et al., 2020b; Liang et al., 2022; Zhou et al., 2023; Wang et al., 2024c),~~
53 ~~chlorine photoactivation (Cao et al., 2024), and enhanced chlorine and photosensitization~~
54 ~~chemistry (Zhang and Chan, 2024) have been proposed. Despite extensive investigations into~~
55 ~~sulfate formation mechanisms, a substantial disparity persists between modeled simulations and~~
56 ~~measured sulfate concentrations, especially in marine boundary layer (Wyant et al., 2015) and~~
57 ~~anthropogenic emission dominated (Wang et al., 2014), highlighting the importance to further~~
58 ~~study the sulfate formation mechanism in these areas.~~

59 ~~Biomass burning (BB) emits around 34–41 Tg of smoke aerosol annually, making it a significant~~
60 ~~contributor to both gaseous and particulate pollutants like SO₂, primary organic aerosol (POA),~~
61 ~~black carbon (BC) and brown carbon (BrC) (Schill et al., 2020; Laskin et al., 2015; Lin et al.,~~
62 ~~2016; Huang et al., 2022b). The recent Recent fire outbreaks in areas like Canada, Amazonia,~~
63 ~~and Southeast Australia, together with the increased fire frequency and intensity reports in areas~~
64 ~~like western US have highlighted the risks of fire, especially biomass burning (BB), to human~~
65 ~~and animal health and climate change (Bond et al., 2013; Andreae, 2019; Jones et al., 2022).~~
66 ~~As an agricultural powerhouse, China boasts immense agricultural crop yields, especially in~~
67 ~~rice, wheat, and corn throughout the country. These crop residues are frequently burned in rural~~
68 ~~areas for cooking and heating purposes, as well as for land preparation after harvest, resulting~~
69 ~~in the substantial production of light-absorbing species, such as brown carbon (BrC) (Chen et~~
70 ~~al., 2017). Atmospheric processes, e.g., atmospheric aging or long-range transport, can alter the~~
71 ~~chemical compositions and optical properties of BrC, potentially affecting the global climate.~~
72 ~~Recent studies have reported that the specific BrC species from biomass burning, including e.g.,~~
73 ~~vanillin (VL), acetovanillone, syringaldehyde (SyrAld), can act as photosensitizers (PS) and~~
74 ~~oxidize SO₂ to sulfate (Zhou et al., 2023; Liang et al., 2024). Atmospheric processes like ,e.g.,~~
75 ~~atmospheric aging or long-range transport, can alter the chemical compositions and optical~~
76 ~~properties of PS-BrC, potentially affecting the sulfate formation potential. the global climate.~~

77 Sea-salt aerosol (SSA), with its high particulate matter loadings and extensive surface area, ~~is~~
78 ~~a crucial atmospheric constituent that~~ plays a significant role in interfacial and multiphase
79 reactions with reactive gases, thereby impacting global radiation balance and air quality in
80 marine and coastal areas (Gantt and Meskhidze, 2013; Chi et al., 2015). Prior research has
81 identified several secondary sulfate formation pathways in SSA, e.g., multiphase SO₂ oxidation
82 by O₃ (Alexander et al., 2012), coexistence of NO₂ (Zhang and Chan, 2023b), PS (Tang et al.,
83 2023), chlorine-PS synergistic effects (Zhang and Chan, 2024), and Cl and OH radicals
84 generated by chlorine photoactivation (Cao et al., 2024), highlighting the importance of NaCl-
85 based photochemistry in sulfate formation.

86 SSA can frequently mix with organic matter through processes such as sea-to-air emission,
87 photochemical oxidation and atmospheric transport (Liu et al., 2023b). Previous studies have
88 observed ~~high elevated~~ sulfate concentrations ~~and light absorption properties~~ in coastal regions
89 when air masses passed through inland areas due to intensive ~~biomass burning~~ or other
90 anthropogenic emissions, suggesting the possible interactions between the ~~sea salt aerosol~~ SSA
91 (primarily sodium chloride) and anthropogenic emissions ~~e.g., biomass burning~~ (Qiu et al.,
92 2019; Huang et al., 2018; Wu et al., 2022). ~~For example, Qiu et al. (2019) discovered high~~
93 ~~absorption Ångström exponent (AAE of 1.46) in coastal city Xiamen, when the air masses~~
94 ~~passing through Southeast Asia with intense biomass burning.~~ Van Pinxteren et al. (2015)
95 observed an increase in sulfate concentration (2.26 µg m⁻³) during the RV MARIA S cruise as
96 it approached the African mainland, in contrast to the marine-origin aerosol (1.59 µg m⁻³),
97 showing significant influence of ~~biomass burning~~. Hence, mixing of sea-salt and biomass
98 burning aerosols can happen in coastal regions.

99 Since the sulfate formation rate depends on the intrinsic properties of the solution matrix and
100 the two main reaction matrixes in marine boundary layer (MBL) were wet aerosol (droplet in
101 our case) and cloud/fog (bulk aqueous), both droplet and aqueous reactions are relevant for
102 studying the aqueous reactions in aerosols and clouds within MBL (Ruiz-Lopez et al., 2020;
103 Herrmann, 2003). Typically, droplet experiments were characterized by high ionic strength (up
104 to >10 M), low liquid water content (10⁻⁷-10⁻³ cm³ m⁻³) and high surface-to-volume ratio
105 whereas aqueous reactions exhibit the opposite characteristics. Transmission electron
106 microscopy (TEM) studies indicate that most coastal particles are internally mixed, showing a
107 higher proportion of organic and salt mixtures in the presence of biomass burning aerosols,
108 accompanied by an increase in sulfate (Dang et al., 2022; Li et al., 2003). However,
109 discrepancies persist between modeled simulations and measured sulfate concentrations in
110 MBL (Yu et al., 2023). The interactions of sea-salt and BB aerosols, especially in multiphase
111 reactions, can potentially unravel the intricate chemistry of sulfate formation in BB affected
112 MBL. Hence, internal mixtures of inorganic salt and water-soluble organic carbons are often
113 used in reaction studies (Tan et al., 2024).

114 ~~However, the studies on interactions of anthropogenic emission and sea salt aerosol on sulfate~~
115 ~~formation are very scarce.~~

116 ~~Prior research has identified several secondary sulfate formation pathways in sea-salt aerosol,~~
117 ~~e.g., multiphase SO₂ oxidation by O₃ (Alexander et al., 2012), coexistence of NO₂ (Zhang and~~
118 ~~Chan, 2023b), photosensitizers (Tang et al., 2023), chlorine photosensitizer synergistic effects~~

119 (~~Zhang and Chan, 2024~~), and Cl and OH radicals generated by chlorine photoactivation (~~Cao~~
120 ~~et al., 2024~~), highlighting the importance of NaCl-based photochemistry in sulfate formation.
121 Our prior study observed higher sulfate formation for incense burning NaCl particles than pure
122 NaCl particles (~~Tang et al., 2023~~). The follow-up research found magnitudes higher sulfate
123 formation rate ($\sim 132 \mu\text{M s}^{-1}$) in premixed $\text{NH}_4\text{Cl}+\text{IC}$ (imidazole 2-carboxaldehyde, a model
124 photosensitizer found in secondary organic aerosol) particles than pure NH_4Cl particles (~ 1.8
125 $\mu\text{M s}^{-1}$) (~~Zhang and Chan, 2024~~). ~~However, the studies on interactions of anthropogenic~~
126 ~~emission and sea salt aerosol on sulfate formation are very scarce.~~

127 In this study, we performed in-situ droplet and aqueous experiments using BB extracts-NaCl
128 mixture to explore the possible interplay between biomass burning and marine aerosols in
129 coastal areas. BB was derived from the burning of rice straw (RS), wheat straw (WS), and corn
130 straw (CS) as well as incense burning (IS). ~~This is supplemented by aqueous reactions using~~
131 ~~BB extracts and bisulfite to mimic the in-cloud aqueous reactions of biomass burning emission-~~
132 ~~mediated S(IV) oxidation. The effects of chloride on sulfate formation were also studied.~~ The
133 aims of this study are to: (i) compare the differences in sulfate formation among different kinds
134 of BB-NaCl particles and BB extracts; (ii) ~~evaluate-examine~~ the impacts of the atmospheric
135 aging (UV-OH• aging) on sulfate formation across different BB-NaCl particles and BB extracts;
136 (iii) investigate ~~Investigating~~ the role of chloride ions in BB extracts mediated sulfate formation.

137 **2 Material and methods**

138 **2.1 Burning experiments**

139 Three types of commonly used biomass (RS, WS and CS) were cut into small, uniform pieces
140 (~ 10 cm in length) and dried. About 100 g of the dried biomass materials ($\sim 10\%$ moisture
141 content) was then introduced into a traditionally iron stove commonly used in rural areas
142 (Figure S1). The stove was covered with a hood and the biomass was ignited using a propane
143 lighter. The generated BB smoke was collected onto 90-mm quartz filters at $0.9 \text{ m}^3 \text{ min}^{-1}$ for 10
144 minutes by a custom-made aerosol sampler under mixed combustion condition (include flaming
145 and smoldering, modified combustion efficiency MCE, $0.85 \leq \Delta[\text{CO}_2]/(\Delta[\text{CO}_2]+\Delta[\text{CO}]) \leq$
146 0.95) (Ting et al., 2018). The sampler was placed at a height of 1 meter above the ground and
147 connected to a $\text{PM}_{2.5}$ sampling head through a sampling pump. For incense burning (IS),
148 laboratory generated smoldering smoke was collected on 47-mm quartz filters at a flow rate of
149 $\sim 6.0 \text{ L min}^{-1}$ for 80 min using a stainless-steel combustion chamber. Note that the different
150 combustion modes of IS and BB are intentionally used to represent the real-world combustion
151 conditions. Our previous study demonstrated that IS was representative of BB based on GC \times GC
152 chromatograms and pixel-based partial least squares discriminant analysis ~~Our previous study~~
153 ~~has demonstrated the similarities (especially in sugars such as levoglucosan and phenols) in~~
154 ~~GC \times GC chromatograms between BB and IS~~ (Tang et al., 2023). Hereafter, we will use BB to
155 represent both the real BB materials and the surrogate materials (IS) unless otherwise specified.
156 After sampling, the collected BB samples (fresh BB) were wrapped by pre-baked aluminum
157 foil (550°C for 6 h) and stored at -20°C until further analysis.

158 To achieve atmospheric OH• aging, the collected fresh BB filter samples were put into placed
159 in a the pre-flushed (zero air, more than 24 h) combustion chamber (zero air, more than 24 h)

160 and illuminated ~~under~~ with UV lamps for 40 min. We used lamps of 185 nm and 254 nm, the
161 combination of which have been widely used in oxidation flow reactor design and experiments
162 for mimicking atmospheric OH• concentrations (Peng and Jimenez, 2020; Rowe et al., 2020;
163 Tkacik et al., 2014; Hu et al., 2022). The estimated OH exposure was $\sim 2.0 \times 10^{12}$ molecules
164 cm^{-3} s, equivalent to an atmospheric aging period of 15 days (assuming an average atmospheric
165 OH concentration of 1.5×10^6 molecules cm^{-3}) (Mao et al., 2009). Detailed characterization of
166 the OH exposure can be found in our previous study (Tang et al., 2023).

167 2.2 Materials and instrumentation

168 Aqueous stock solutions of BB samples were prepared by dissolving the collected filters in
169 ultrapure water and subjecting them to ultrasonication in a cooled-water bath three times, each
170 for 20 minutes. The resulting water extracts of the BB were then filtered through 0.22 μm PTFE
171 filters and stored in brown vials at 4°C in a refrigerator. The anions, i.e., chloride, sulfate and
172 nitrate of the BB extracts were analyzed by Dionex ion chromatography (ICS 1100, CA). An
173 aliquot (~ 0.5 ml) of the BB or IS extracts were used for water-soluble organics detection by
174 ultra-high performance liquid chromatography (Thermo Scientific Dionex UltiMate 3000
175 UHPLC) coupled with high-resolution Orbitrap Fusion Lumos Tribrid mass spectrometry
176 (Orbitrap HRMS, Thermo Fisher Scientific, USA). The particulate organic matter was also
177 characterized by a thermal desorption module (TDS3, Gerstel) coupled to comprehensive two-
178 dimensional gas chromatography-mass spectrometer (GCMS-TQ™8050 NX, Shimadzu,
179 Japan). UV-Vis spectrometry (UV-3600, Shimadzu, Japan) was employed to examine the
180 absorbance of BB extracts. Total organic carbon (TOC) was measured by total carbon analyzer
181 (TOC-L CPH, Shimadzu, Japan). Metal concentrations were measured by inductively coupled
182 plasma-mass spectrometry (ICP-MS, Agilent 7800). Detailed analysis can be found in Text S1.
183 Aqueous stock solution of sodium chloride ($\geq 99.8\%$, Unichem) was prepared by dissolving the
184 corresponding salt in ultrapure water to obtain a concentration of 1M. The study utilized high
185 purity grade synthetic air and nitrogen supplied by the Linde HKO Ltd., while sulfur dioxide
186 was obtained from the Scientific Gas Engineering Co., Ltd.

187 2.3 Multiphase and aqueous-phase reactions of S(IV)

188 ~~For~~ In SO₂ uptake experiments, the stock solution of BB extracts was premixed with sodium
189 chloride solution (1M) at a volume ratio of 1:1 and the solutions had pH a of 4-6. A droplet
190 generator (Model 201, Uni-Photon Inc.) was then utilized to ~~generate droplets, which were~~
191 subsequently deposited droplets onto a hydrophobic substrate (model 5793, YSI Inc.) for SO₂
192 uptake experiments. Reactive SO₂ uptake experiments were performed via a flow cell/in-situ
193 Raman system at controlled room temperature (23-25°C). The top and bottom quartz windows
194 of the flow cell were used for Raman analysis and UV irradiation, respectively. The light
195 experiment was performed using a xenon lamp (model 6258, ozone free, 300W, Newport, light
196 intensity of 1318 mW/cm²), with photon flux of 9.8×10^{15} photons cm^{-2} s^{-1} in 280-420 nm
197 received by particles in the flow cell (Zhang and Chan, 2023b). Identical experiments were
198 conducted in the dark, with the lights off and the experimental area kept in complete darkness.
199 The relative humidity (RH) inside the flow cell was adjusted to 80% by mixing dry and wet
200 synthetic air or nitrogen. The particles were then equilibrated at 80% RH for over 60 min and
201 remained liquid throughout the experiment period. SO₂ was introduced into the system to reach

202 a concentration of 8.0 ppm. The prescribed size used in our in-situ Raman research was 60 ± 5
203 μm . Despite using particles for droplet experiments that were larger than ambient fine particles,
204 we employed the SO_2 uptake coefficient (γ_{SO_2}) as a kinetic parameter to account for the particle
205 size effects. Comprehensive calculation of γ_{SO_2} can be found in our previous studies (Gen et
206 al., 2019b, a; Tang et al., 2023; Zhang et al., 2020a).

207 Aqueous-phase photochemical reactions were performed using a custom-built quartz photo
208 reactor (Mabato et al., 2023; 2022). Specifically, a 500 mL solution containing 100 ppm
209 bisulfite and 1 ppm BB TOC extracts were continuously mixed using a magnetic stirrer
210 throughout the experiments. Note that the 1 ppm BB TOC and 100 ppm bisulfite align well
211 with the atmospheric-relevant ranges in aqueous aerosols, fogs and clouds, where PS
212 concentration can reach hundreds of micromolar and total sulfur concentration can exceed
213 several millimolar. (Anastasio et al., 1997; Guo et al., 2012; Shen et al., 2012; Rao and Collett,
214 1995) To achieve air-saturated conditions, synthetic air was continuously introduced to the
215 solutions at a flow rate 0.5 L min^{-1} throughout the experiments. The above mixed solutions were
216 then exposed to radiation via the same xenon lamp as in the droplet experiments. Samples were
217 collected at 1h interval for a total of 8 h for sulfate and bisulfite analysis using ion
218 chromatography.

219

220 **3 Results and Discussion**

221 **3.1 Enhanced sulfate production of BB-NaCl droplets compared to IS-NaCl droplets.**

222 As no sulfate was detected in the dark conditions for any of the experiments, we have focused
223 on the light experiments. Figure 1 depicts the sulfate production by (a) fresh BB-NaCl; (b) aged
224 BB-NaCl droplets as a function of time in the presence of light, air and SO_2 at 80% RH. As our
225 previous study (Tang et al., 2023) has found significantly higher sulfate formation of IS-NaCl
226 droplets over NaCl droplets, here we only focus on the comparison of sulfate formation between
227 different kinds of BB-NaCl droplets and IS-NaCl droplets. ~~Note that sulfate concentration was~~
228 ~~normalized to the initial TOC concentration of the mixture to facilitate the comparison of sulfate~~
229 ~~production of different droplet compositions.~~ Regardless of whether the extracts were fresh or
230 aged, the sulfate production by real BB-NaCl droplets was higher than IS-NaCl droplets.
231 Specifically, sulfate formed by fresh (F) BB-NaCl droplets followed the trends of $\text{CS}_\text{F}\text{-NaCl}$
232 ($16.8 \pm 2.6 \text{ mM ppmC}^{-1}$) $>$ $\text{RS}_\text{F}\text{-NaCl}$ ($9.8 \pm 0.1 \text{ mM ppmC}^{-1}$) $>$ $\text{WS}_\text{F}\text{-NaCl}$ ($4.2 \pm 0.2 \text{ mM ppmC}^{-1}$)
233 $>$ $\text{IS}_\text{F}\text{-NaCl}$ (0.8 mM ppmC^{-1}) after illumination for 1080 min. In aged (A) samples, while
234 $\text{BB}_\text{A}\text{-NaCl}$ is more efficient than $\text{IS}_\text{A}\text{-NaCl}$ in sulfate formation, the order of sulfate formation
235 was different from the fresh samples: $\text{RS}_\text{A}\text{-NaCl}$ ($35.2 \pm 0.6 \text{ mM ppmC}^{-1}$) $>$ $\text{CS}_\text{A}\text{-NaCl}$ ($13.0 \pm$
236 0.1 mM ppmC^{-1}) $>$ $\text{WS}_\text{A}\text{-NaCl}$ ($6.0 \pm 1.6 \text{ mM ppmC}^{-1}$) $>$ $\text{IS}_\text{A}\text{-NaCl}$ (0.6 mM ppmC^{-1}). The
237 sulfate enhancement factors of $\text{RS}_\text{F}\text{-NaCl}$, $\text{WS}_\text{F}\text{-NaCl}$, and $\text{CS}_\text{F}\text{-NaCl}$ over $\text{IS}_\text{F}\text{-NaCl}$ after 18 h
238 SO_2 uptake ($\text{Sulfate}_{\text{BB}_\text{F}\text{-NaCl}/\text{IS}_\text{F}\text{-NaCl}}$) were 11.7, 5.0 and 20.0, respectively. The enhancement
239 of sulfate can also be observed in aged BB samples, with values of 54.3, 9.2 and 20.1 for $\text{RS}_\text{A}\text{-}$
240 NaCl , $\text{WS}_\text{A}\text{-NaCl}$, and $\text{CS}_\text{A}\text{-NaCl}$, respectively. The lower sulfate formation of IS-NaCl droplets
241 than BB-NaCl droplets can be explained by the significantly higher TOC concentration of IS
242 due to the incomplete and smoldering combustion (Table S1). The TOC concentration of the IS

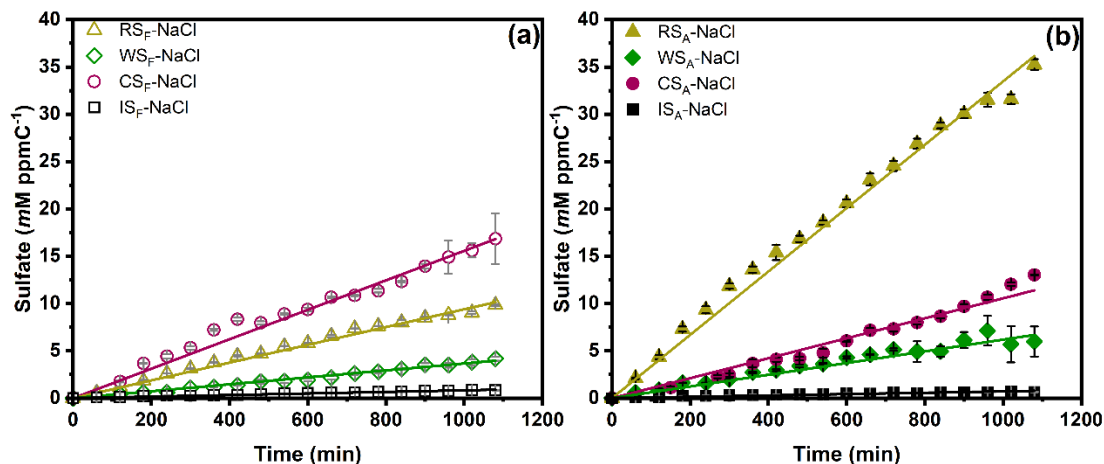
243 extracts ($>550 \text{ mg L}^{-1}$) was nearly an order of magnitude higher than that of the BB extracts
244 ($34.0\text{-}69.9 \text{ mg L}^{-1}$), while WSOC/(WSOC+ Σ anions) exhibited a more than tenfold increase in
245 BB extracts than in IS extracts. Previous studies have confirmed that the smoldering condition
246 of BB will result in significantly more organic compounds and less ions than flaming condition
247 (Wang et al., 2020c; Fushimi et al., 2017; Kalogridis et al., 2018; Kim et al., 2018). Additionally,
248 significantly higher polycyclic aromatic hydrocarbons (PAHs) proportion (12.2%-16.6% by
249 intensity) than IS ($\sim 5.0\%$) were observed by GC \times GC-MS. Huang et al. (2022a) reported higher
250 ~~polyeyelic aromatic hydrocarbons (PAHs)~~ in BB particulates (CS, WS, RS, $>262.5 \text{ mg kg}^{-1}$
251 $>3.7\%$ of organic matter) than in IS particulates (3.3 mg kg^{-1} , 0.9% of organic matter) (Song
252 et al., 2023). Fushimi et al. (2017) and Kim et al. (2021) demonstrated that more PAHs would
253 be emitted under flaming compared to smoldering conditions. PAHs like pyrene, fluoranthene,
254 and phenanthrene have been recognized as PS photosensitizers (Jiang et al., 2021; Yang et al.,
255 2021) and are mainly from combustion processes, e.g., pyrosynthesis from aliphatic and
256 aromatic precursors in biomass burning processes and the constituents vary with temperatures
257 and oxygen contents (Pozzoli et al., 2004). The higher percentage of PAHs in BB together with
258 the collection procedure (mixed combustion and higher temperature for real BB while
259 smoldering and lower temperature for IS) suggested the BB materials would generate more
260 PAHs at high temperatures and may contribute to sulfate formation.

261 Table 1 and Figure S2 presents the reactive (γ_{SO_2}) and normalized reactive SO_2 uptake
262 coefficients ($n\gamma_{\text{SO}_2}$) of different BB-NaCl droplets. The γ_{SO_2} obtained in our study are $0.9 -$
263 6.6×10^{-6} , which are consistent but fall on the low side of the reported heterogeneous SO_2
264 oxidation processes, including nitrate photolysis ($10^{-6}\text{-}10^{-5}$) (Gen et al., 2019b), TMI-catalyzed
265 oxidation ($10^{-6}\text{-}10^{-4}$) (Zhang et al., 2024), NO_2/O_3 oxidation ($10^{-6}\text{-}10^{-4}$) (Zhang et al., 2021a;
266 Zhang and Chan, 2023a) and peroxide oxidation ($10^{-6}\text{-}10^{-1}$) (Wang et al., 2021a; Ye et al., 2018;
267 Yao et al., 2019). Additionally, the reported γ_{SO_2} in our study aligns well with the results
268 obtained from ambient samples in Beijing (Zhang et al., 2020b). The large discrepancy of the
269 reported γ_{SO_2} can be attributed to the differences in aerosol components, particle size, RH, SO_2
270 and oxidants concentrations. From our results, it appears that sulfate formation from BB-
271 NaCl particles is much less effective than particles under nitrate photolysis. It is interesting
272 to note that Zhou et al. (2023) found particles coated with model PS compounds much more
273 effective in sulfate formation than nitrate particles under photolysis in a PAM reactor. The
274 much shorter residence time in that reactor (2.5 min) and higher PS concentration ($\sim 66 \text{ mM}$)
275 than the exposure time of filter samples (40 min) and PS concentration ($<250 \text{ ppm}$) in our
276 sulfate experiments may explain the differences in the comparison of PS/BB and nitrate
277 photolysis results. Higher $n\gamma_{\text{SO}_2}$ were found for fresh and aged real BB-NaCl than IS-NaCl
278 droplets, following the trend of : $\text{CS}_F\text{-NaCl}$ ($8.8 \times 10^{-8} \text{ ppmC}^{-1}$) $>$ $\text{RS}_F\text{-NaCl}$ ($6.2 \times 10^{-8} \text{ ppmC}^{-1}$)
279 $>$ $\text{WS}_F\text{-NaCl}$ ($2.0 \times 10^{-8} \text{ ppmC}^{-1}$) $>$ $\text{IS}_F\text{-NaCl}$ ($0.61 \times 10^{-8} \text{ ppmC}^{-1}$) and $\text{RS}_A\text{-NaCl}$ (2.2×10^{-7}
280 ppmC^{-1}) $>$ $\text{CS}_A\text{-NaCl}$ ($6.2 \times 10^{-8} \text{ ppmC}^{-1}$) $>$ $\text{WS}_A\text{-NaCl}$ ($3.5 \times 10^{-8} \text{ ppmC}^{-1}$) $>$ $\text{IS}_A\text{-NaCl}$ (0.46×10^{-8}
281 ppmC^{-1}), respectively.

282 In our previous study, we observed a significant increase in sulfate formation for IS-NaCl
283 droplets than NaCl droplets, which we attributed to photosensitization (Tang et al., 2023).
284 Considering the fact that BB-NaCl droplets produced sulfate more efficiently than IS-NaCl
285 droplets and NaCl droplets, we explore the underlying mechanisms driving this phenomenon.

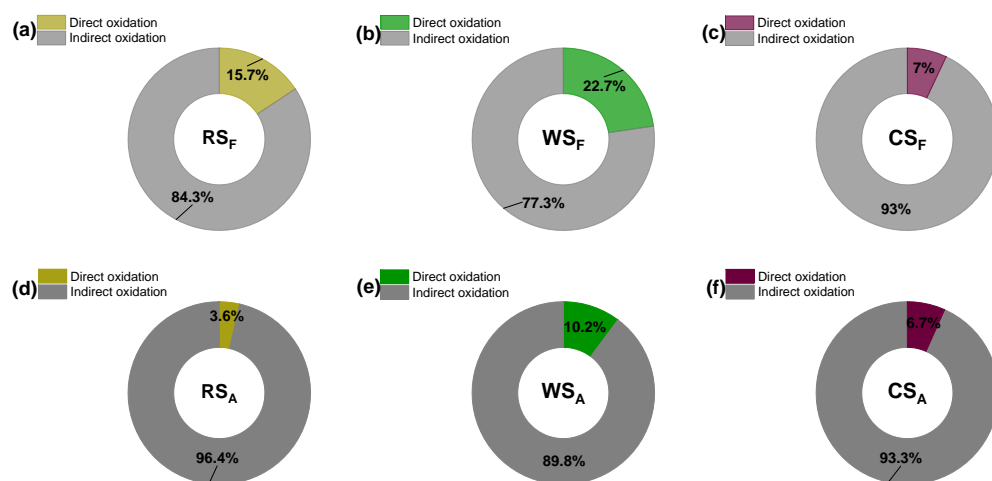
286 Possible reasons include nitrate (from BB extracts or newly formed) photolysis, $[\text{Cl}^- \cdot \text{H}_3\text{O}^+ \cdot \text{O}_2]$
287 photoexcitation (Cl^- from BB extracts), H_2O_2 oxidation, BC-catalyzed oxidation, reactive
288 nitrogen species oxidation, and organics-driven pathways e.g., HCHO, photosensitizing
289 components, organic peroxide, and TMI-organic oxidation (Ye et al., 2023).

290 Since there was no nitrate peak in our Raman spectra in all experiments, the potential impact
291 from nitrate photolysis was excluded. Besides, the significantly low Cl^- concentration (0.0002-
292 0.001M) in the original BB extracts (compared to 1M NaCl, Table S1) has minimized the
293 influence of chloride photoexcitation of $[\text{Cl}^- \cdot \text{H}_3\text{O}^+ \cdot \text{O}_2]$ (Cl^- from BB extracts) on the sulfate
294 formation. Reactive nitrogen species e.g., NO_x , HONO and NH_3 were neither introduced nor
295 detected in our system, indicating that the oxidation pathway involving reactive nitrogen
296 species was insignificant. Additionally, the water extraction process has excluded the possibility
297 of BC-catalyzed oxidation. The absence of sulfate formation in dark conditions ruled out the
298 involvement of direct H_2O_2 oxidation and organic peroxide oxidation pathways. The
299 concentrations of TMI did not exhibit a consistent relationship with the sulfate formation
300 observed in both $\text{BB}_F\text{-NaCl}$ and $\text{BB}_A\text{-NaCl}$ droplets (Figure S2S3), suggesting that the TMI-
301 catalyzed oxidation pathway may not be responsible for the observed phenomenon. Therefore,
302 the most probable reason for the enhancement of sulfate formation by BB-NaCl droplets over
303 NaCl droplets would be the photosensitizing components. Given the complexity and the lack
304 of a method to quantify PS in BB aerosols, using the total TOC concentration as an upper limit
305 for estimating PS concentration is considered a compromise that allows for systematic
306 comparison. Our goal is to compare the photosensitizing ability in different chemical
307 systems, but not to quantify their absolute values. Therefore, the sulfate formation reported
308 here can be considered as the lower limit of photosensitizing capacity. State-of-the-art mass
309 spectrometry analysis including UHPLC-Orbitrap-MS and GC×GC-MS showed the existence
310 of possible photosensitizers-PS such as PAHs (e.g., fluoranthene, pyrene, cyclopenta[cd]pyrene,
311 4-methylphenanthrene, benzo[a]pyrene, perylene, Table S2) and aromatic carbonyls (SyrAld,
312 VL, 3,4-dimethoxybenzaldehyde, acetophenone, acetosyringone, Table S2). Photosensitizing
313 components can directly or indirectly (by forming secondary oxidants in the presence of oxygen)
314 oxidize S(IV) to S(VI). Wang et al. (2020b) proposed a direct oxidation process of S(IV) to
315 sulfate by excited triplet states of photosensitizers ($^3\text{PS}^*$). To explore the contribution of the
316 direct $^3\text{PS}^*$ oxidation on sulfate formation, we performed the same sets of experiments in N_2 -
317 saturated condition, shown in Figure S32. Under N_2 -saturated conditions, secondary oxidants
318 such as $\text{HO}_2\cdot$, $\text{OH}\cdot$ oxidation pathway can be ruled out due to the lack of oxygen. Consequently,
319 the sulfate formed under this condition can be considered as the direct PS^* oxidation. The BB-
320 NaCl droplets showed only direct PS^* oxidation contribution of 3.6% to 22.7%, highlighting
321 the predominant role of secondary oxidants (Tang et al., 2023). For $\text{BB}_F\text{-NaCl}$ droplets, the
322 contribution of direct PS^* followed the trend of $\text{WS}_F\text{-NaCl}$ (22.7%) > $\text{RS}_F\text{-NaCl}$ (15.7%) >
323 $\text{CS}_F\text{-NaCl}$ (7.0%), while for $\text{BB}_A\text{-NaCl}$ droplets, $\text{WS}_A\text{-NaCl}$ (10.2%) > $\text{CS}_A\text{-NaCl}$ (6.7%) >
324 $\text{RS}_A\text{-NaCl}$ (3.6%) was observed. In summary, regardless of whether fresh or aged, the
325 secondary oxidants triggered by indirect PS^* oxidation were the main reason for sulfate
326 formation, highlighting the importance of O_2 in PS^* mediated oxidation processes.



327

328 Figure 1. Sulfate production under different droplet compositions as a function of time by
 329 droplet experiments: (a) fresh BB-NaCl droplets; (b) aged BB-NaCl droplets in air at 80% RH.
 330 RS, WS, CS and IS represent rice straw, wheat straw, corn straw and incense burning,
 331 respectively. The subscripts F and A represent fresh and aged, respectively.



332

333 Figure 2 Contributions of direct and indirect PS* oxidation to sulfate in droplet experiments

334 Table 1. Sulfate formation rate constant ($k_{SO_4^{2-}}$), reactive (γ_{SO_2}) and normalized SO_2 uptake
 335 coefficient ($n\gamma_{SO_2}$) of various particle compositions at 80% RH. Sulfate formation rate ($k_{SO_4^{2-}}$)
 336 for aqueous phase reactions using different BB extracts and model compounds. 1, 10, 100 and
 337 200 represent the concentration of different compounds (in ppm).

Particle Composition	$k_{SO_4^{2-}}$ ($\mu\text{M min}^{-1} \text{ppmC}^{-1}$)	γ_{SO_2}	$n\gamma_{SO_2}$ ^a ppmC ⁻¹
RS _F -NaCl	9.4 ± 0.10	$(2.2 \pm 0.023) \times 10^{-6}$	$(6.2 \pm 0.066) \times 10^{-8}$
WS _F -NaCl	3.7 ± 0.048	$(0.66 \pm 0.0086) \times 10^{-6}$	$(2.0 \pm 0.027) \times 10^{-8}$
CS _F -NaCl	15.6 ± 0.11	$(2.0 \pm 0.015) \times 10^{-6}$	$(8.8 \pm 0.065) \times 10^{-8}$

IS _F -NaCl	0.83 ± 0.011	(1.7 ± 0.034) × 10 ⁻⁶	(0.61 ± 0.012) × 10 ⁻⁸
RS _A -NaCl	33.5 ± 0.38	(6.6 ± 0.074) × 10 ⁻⁶	(21.5 ± 0.24) × 10 ⁻⁸
WS _A -NaCl	6.2 ± 0.18	(0.92 ± 0.027) × 10 ⁻⁶	(3.5 ± 0.10) × 10 ⁻⁸
CS _A -NaCl	10.6 ± 0.23	(1.0 ± 0.023) × 10 ⁻⁶	(6.2 ± 0.13) × 10 ⁻⁸
IS _A -NaCl	0.72 ± 0.026	(1.3 ± 0.052) × 10 ⁻⁶	(0.46 ± 0.017) × 10 ⁻⁸
Aqueous Reactions	Concentration (ppm)	$k_{so_4^-}$ (ppm min ⁻¹)	$k_{so_4^{2-}^a}$ (μM min ⁻¹)
RS _F	1	0.31	3.2
RS _F -NaCl	1-100	0.16	1.6
RS _F -NaCl	1-200	0.085	0.9
WS _F	1	0.19	2.0
CS _F	1	0.25	2.6
IS _F	1	0.19	2.0
RS _A	1	0.33	3.4
RS _A -NaCl	1-100	0.37	3.8
RS _A -NaCl	1-200	0.63	6.4
WS _A	1	0.26	2.7
CS _A	1	0.33	3.4
IS _A	1	0.080	0.82
NaCl	100	0.051	0.52
NaCl	200	0.079	0.81
SyrAld	1	0.15	1.5
SyrAld-Pyz	1-1	0.68	7.1
SyrAld-Pyz-NaCl	1-1-10	0.67	6.9
SyrAld-Pyz-NaCl	1-1-100	0.55	5.7
SyrAld-Pyz-NaCl	1-1-200	0.50	5.2
SyrAld-4-NC	1-1	0.11	1.1
SyrAld-4-NC-NaCl	1-1-10	0.13	1.4
SyrAld-4-NC-NaCl	1-1-100	0.13	1.4

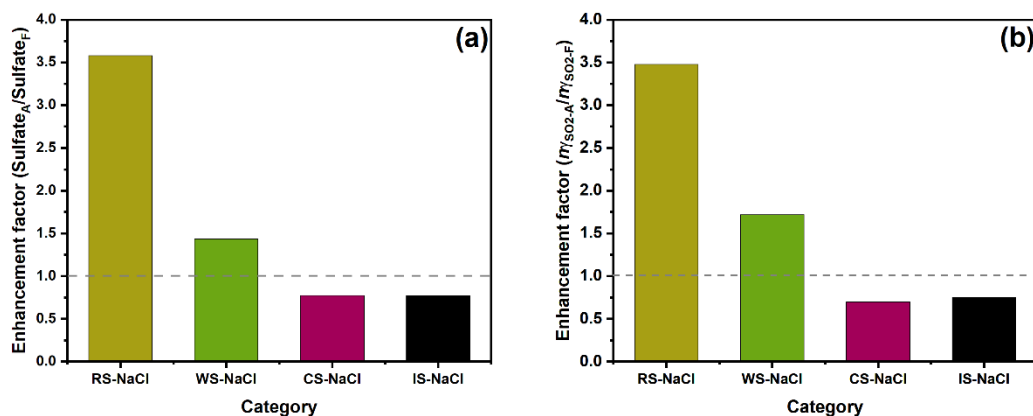
SyrAld-4-NC- NaCl	1-1-200	0.15	1.5
SyrAld-NaCl	1-10	0.11	1.1
SyrAld-NaCl	1-100	0.17	1.8
SyrAld-NaCl	1-200	0.17	1.7
VL	1	0.26	2.7
VL-Pyz	1-10	0.61	6.4
VL-Pyz-NaCl	1-1-10	0.55	5.8
VL-Pyz-NaCl	1-1-100	0.43	4.5
VL-Pyz-NaCl	1-1-200	0.42	4.3
VL-4-NC	1-1	0.17	1.7
VL-4-NC-NaCl	1-1-10	0.22	2.3
VL-4-NC-NaCl	1-1-100	0.27	2.7
VL-4-NC-NaCl	1-1-200	0.23	2.4
VL-NaCl	1-10	0.25	2.6
VL-NaCl	1-100	0.26	2.7
VL-NaCl	1-200	0.28	2.9

^aThe $n\gamma_{SO_2}$ was calculated by normalizing the γ_{SO_2} with the TOC concentration in the BB extracts was normalized by the initial TOC concentration (ppmC), i.e., $n\gamma_{SO_2} = \gamma_{SO_2}/TOC$

338

339 3.2 Aging effects on sulfate formation across various BB materials

340 To investigate the aging effects across various BB materials, we ~~aged~~ subjected the collected
341 BB filters to OH radical aging by irradiating them with UV lights at wavelengths of (185 nm
342 and 254 nm). This combination effectively generate OH radicals (Tang et al., 2023). Figure S4
343 exhibits the differences in sulfate formation rates of different fresh and aged BB materials. RS
344 and WS show sulfate formation enhancement, while CS and IS show reduction after aging.
345 Figure 23(a) shows that the 18h sulfate enhancement factor ($Sulfate_A/Sulfate_F$) followed the
346 trend of RS-NaCl (3.6) > WS-NaCl (1.4) > CS-NaCl (0.8) \approx IS-NaCl (0.8), which is neither
347 consistent with the trends of sulfate formation for BB_F -NaCl nor BB_A -NaCl, indicating that
348 aging processes have different influence on sulfate formation towards BB materials. A similar
349 trend was found for $n\gamma_{SO_2}$, showing the highest and lowest sulfate enhancement for RS-NaCl
350 (3.5) and IS-NaCl (0.7), respectively.



351

352 Figure 23. Enhancement factor of (a) sulfate and (b) normalized SO₂ uptake coefficient $n\gamma_{SO_2}$
 353 between fresh and aged BB-NaCl droplets by droplet experiments.

354 ~~We also performed aqueous reactions using fresh/aged BB extracts to investigate the aging~~
 355 ~~effects on the sulfate formation (Figure S7). The sulfate formation rate ($k_{SO_4^{2-}}$) for different BB~~
 356 ~~extracts during initial photoinduced experiments ranged from 0.8 to 3.4 $\mu\text{M min}^{-1}$. The $k_{SO_4^{2-}}$~~
 357 ~~obtained in bulk phase reactions were a magnitude lower than that of the droplets (Table 1);~~
 358 ~~which is consistent with previous studies (Wang et al., 2024c; Zhang and Chan, 2024). Wang~~
 359 ~~et al. (2024c) discovered sulfate formation rate magnitudes higher at air-water interface (AWI)~~
 360 ~~than conventional bulk phase reactions. They attributed this to accelerated electron transfer~~
 361 ~~process at AWI, where $^3\text{PS}^*$ ($^3\text{HULIS}^*$ in their case) can accept electrons from HSO_3^- in a more~~
 362 ~~efficient way due to their incomplete solvent cages. Zhang and Chan (2024) fitted a 3 orders~~
 363 ~~of magnitude higher rate constant of IC^*+Cl^- ($\sim 10^8 \text{ M}^{-1}\text{s}^{-1}$) in particle phase than bulk phase~~
 364 ~~rate constant ($\sim 10^5 \text{ M}^{-1}\text{s}^{-1}$) (Gemayel et al., 2021; Woods et al., 2020). They attributed the~~
 365 ~~enhanced sulfate formation to the expedited reactions between $^3\text{PS}^*$ and chloride ions to form~~
 366 ~~reactive chlorine species, facilitated by the decreased solvation of chloride and $^3\text{PS}^*$ at the AWI~~
 367 ~~(Zhang and Chan, 2024). Many studies have demonstrated that chloride ions, bisulfite ions and~~
 368 ~~surfactant-like PS have the propensity to reside at the AWI of droplets, primarily driven by~~
 369 ~~polarization interactions. This promotes enlarged bond dipole moments and ordered alignment~~
 370 ~~of reactant molecules, resulting in reduced entropy and heightened free energy of the initial~~
 371 ~~state (Jungwirth and Tobias, 2002, 2006; Ruiz-Lopez et al., 2020; Tinel et al., 2016; Yan et al.,~~
 372 ~~2016; Fu et al., 2015). Other factors, e.g., S(IV) concentration (8 ppm gaseous SO₂ in droplet~~
 373 ~~experiment and 100 ppm HSO_3^- in aqueous reactions), and the addition of NaCl (1M NaCl~~
 374 ~~addition in droplets and no NaCl addition in aqueous reactions) may also contribute to the high~~
 375 ~~sulfate formation rate in droplet experiments. In this study, the more efficient sulfate formation~~
 376 ~~in droplet experiments than bulk solutions can potentially be attributed to the accelerated~~
 377 ~~reactions induced by photosensitizers at the AWI, intensity variance in droplets and aqueous~~
 378 ~~solution, concentrations difference in S(IV) and the addition of NaCl. However, the detailed~~
 379 ~~mechanisms of the accelerated sulfate formation in droplets than bulk are still uncertain and out~~
 380 ~~of the scope of this paper, and more research should be performed in the future.~~

381 Aqueous reactions using fresh/aged BB extracts were performed to investigate the aging effects
 382 on the sulfate formation in cloud phase (Figure S5). As the experiment proceeded, sulfate

383 concentrations accumulated while bisulfite concentrations decreased. Concurrently, the pH of
384 the aqueous solution decreased from approximately 5.0 to 3.0, reflecting enhanced acidity. In
385 bulk experiments, all BB extracts have higher $k_{SO_4^{2-}}$ after aging. The increased sulfate
386 formation of BB extracts after aging may be due to changes in their chemical compositions.
387 Compared to RS_F (28.3% for CHON- and 67.3% for CHN+ in total intensity), RS_A has higher
388 CHON- (36.1%) and CHN+ (88.3%) percentages (Figs. S6-S7). Zhao et al. (2022) observed a
389 slight increase in CHON percentage for RS from 53.4% to 56.2% after aging. Similar trend was
390 observed for CS extracts, where CHON- and CHN+ percentage increases from 26.7% and 65.2%
391 to 31.5% and 68.8%, respectively, after aging. Given the presence of chromophoric compounds
392 in BrCAs chromophoric compounds are present in brown carbon (BrC) (Laskin et al., 2015),
393 we constrained the DBE values to the range of $\{0.5 \leq DBE \leq 0.9\}$ to semi-qualitatively
394 distinguish BrC chromophores in the dissolved organic carbon BrC (Lin et al., 2018). $BB_{F/A}$
395 was defined as the water-soluble organic species while $BB_{F/A-BrC}$ represented the molecularly
396 identified water-soluble brown carbon falling in the range of $0.5 \leq DBE \leq 0.9$ in BB extracts.
397 These definitions will be consistently applied hereafter. Higher amounts of CHON- species
398 were found in RS_{A-BrC} (41.9%) and CS_{A-BrC} (35.5%) than RS_{F-BrC} (32.3%) and CS_{F-BrC} (34.7%).
399 One of the key categories of CHON- is nitrated aromatics, which have been widely identified
400 in lab-generated BB smoke (Huang et al., 2022b; Wang et al., 2017a; Zhang et al., 2022; Xie et
401 al., 2019) and field campaigns (Salvador et al., 2020; Mohr et al., 2013; Chen et al., 2022). A
402 series of CHON- species, e.g., $C_6H_5NO_3$, $C_6H_5NO_4$, $C_7H_7NO_3$, and $C_8H_9NO_3$, which were
403 tentatively identified as nitrophenol, nitrocatechol, methyl-nitrophenol, and dimethyl-
404 nitrophenol, have been detected in our BB extracts. Nitrophenols photolysis has been found to
405 be a potential source of OH radicals (Sangwan and Zhu, 2018; Guo and Li, 2023; Cheng et al.,
406 2009; Sangwan and Zhu, 2016). Therefore, the increase in sulfate formation by RS_A and CS_A
407 may partially be related to the more oxidants generated by nitrophenol photolysis.

408 Approximately 80% of the CHN+ species identified exhibited a diatomic nitrogen composition
409 in their molecular formula. The precise determination of the molecular structures of these
410 compounds solely based on elemental composition is challenging due to the presence of stable
411 isomers. However, the N-bases, which contain two nitrogen atoms, can be attributed to various
412 N-heterocyclic alkaloids (Figure S8). For example, homologs of $C_5H_6N_2(CH_2)_n$ were likely
413 pyrazine, pyrimidine or amino pyridine, which were composed of six-membered heterocyclic
414 rings with N atoms and alkyl side chains (Lin et al., 2012; Laskin et al., 2009). $C_5H_8N_2(CH_2)_n$
415 were likely alkyl-substituted imidazole compounds, featuring a five-membered heterocyclic
416 ring with two nitrogen atoms as the core structure and alkyl side chains (Lin et al., 2012; Laskin
417 et al., 2009). For $C_7H_6N_2(CH_2)_n$ homologs, the core skeleton was $C_7H_6N_2$, with an AI_{mod} of 0.8,
418 indicating its distinctive characteristics of compounds containing fused five-membered and six-
419 membered rings, such as benzimidazole or indazole (Wang et al., 2017b). Redox-inactive
420 heterocyclic nitrogen-containing bases, e.g., pyridine, imidazole, and their derivatives, have
421 been shown to enhance the redox activity of humic-like substances (HULIS) fraction by
422 hydrogen-atom transfer, with the degree of enhancement directly correlated to their
423 concentration (Dou et al., 2015; Kipp et al., 2004). Thus, the increased CHN+ percentage may
424 also contribute to the enhanced sulfate formation of RS_A and CS_A by acting as a H-bond
425 acceptor to facilitate the $^3PS^*$ -mediated oxidation by generating more oxidants.

426 However, the CHON- and CHN+ percentages in WS_A were lower than WS_F, indicating that the
427 sulfate enhancement in WS_A was not due to the CHON and CHN species. Instead, CHO-
428 accounted for higher proportion in WS_A (68.5%) and WS_{A-BrC} (68.9%) than WS_F (65.0%) and
429 WS_{F-BrC} (64.8%). This aligns with a prior AMS study, showing increased CHO proportions in
430 aged wheat burning emissions (Fang et al., 2017). We suppose that CHO- compounds,
431 particularly photosensitizing compounds with carbonyl groups, would explain the difference of
432 sulfate formation in WS extracts (Gómez Alvarez et al., 2012; Mabato et al., 2023; Felber et al.,
433 2020; Fu et al., 2015). Therefore, we filtered the chemical formula of CHO- species from
434 UHPLC-Orbitrap-HRMS by applying the maximum carbonyl ratio (MCR) (Zhang et al., 2021b;
435 Wang et al., 2024a; Calderon-Arrieta et al., 2024; Liu et al., 2023a), H/C, O/C as well as
436 modified aromaticity index (AI_{mod}) to focus on potential ~~photosensitizers-PS~~ (Zherebker et al.,
437 2022; Koch and Dittmar, 2006). In short, molecular formula were classified into six groups,
438 namely, condensed aromatics (AI_{mod}≥0.67), polyphenolics (0.50<AI_{mod}<0.67), highly
439 unsaturated and phenolic compounds (AI_{mod}≤0.5, H/C<1.5), aliphatics (H/C≥1.5, O/C≤0.9,
440 N=0), peptide-like compounds (H/C≥1.5, O/C≤0.9, N>0) and sugar-like compounds (H/C≥1.5,
441 O/C>0.9), details can be found in Text S1. As aliphatics, peptide-like compounds and sugar-
442 like compounds are unlikely to be ~~PSphotosensitizers~~, we exclude them as potential PS. By
443 applying a data filtration process involving CHO-, condensed aromatics, polyphenolics, highly
444 unsaturated and phenolic compounds based on the mentioned criteria ~~above-mentioned,~~
445 ~~and as well as~~ MCR≥0.9 (which includes oxidized unsaturated and highly unsaturated
446 compounds such as PS like imidazole-carboxaldehyde and PAHs) (Zhang et al., 2021b), 52.6%
447 and 49.7% of the compounds (by intensity) can be considered as potential PS in ~~were selected~~
448 ~~by~~ WS_A and WS_F, respectively. The main compositional difference lies in polyphenolics,
449 comprising 26.3% and 21.8% of WS_A and WS_F respectively. Therefore, the higher sulfate
450 formation in WS_A may be related to the higher contributions of the polyphenolics, e.g., C₈H₈O₃.

451 To summarize, we propose that the enhanced sulfate formation in CS_A and RS_A was likely due
452 to the increased proportions (by intensity) of CHON and CHN species, potentially nitrophenols
453 and N-heterocyclic compounds. Conversely, the increased sulfate formation in WS_A appears to
454 be linked to a higher percentage of CHO species. However, the associations between detailed
455 chemical characteristics and sulfate formation were not provided in this study due to the
456 complexity of the interactions between different chemical categories and difficulties in the
457 interpretation of the coefficients. Future studies are needed to elucidate the relationships
458 between sulfate formation and the chemical characteristics.

459

460 3.3 Effects of Chloride and Nitrogen-containing Species on Sulfate Formation

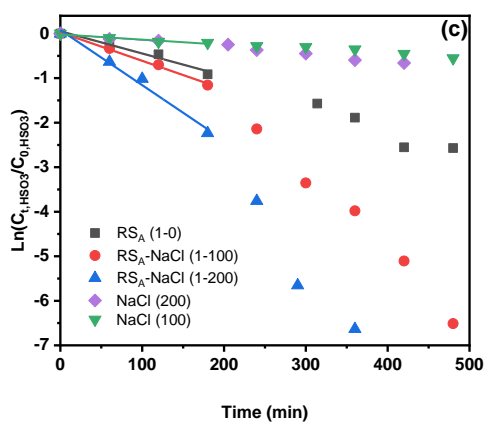
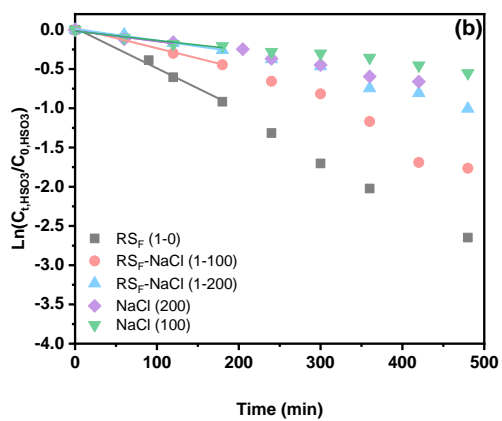
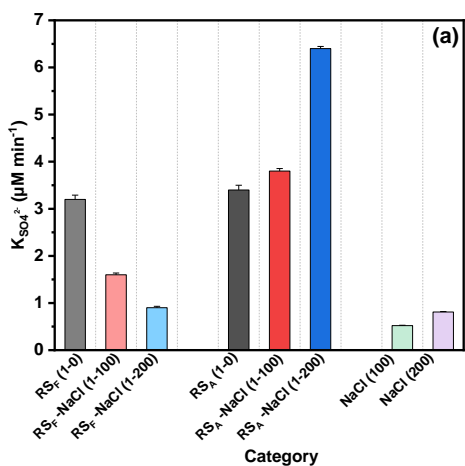
461 Unlike the droplet experiments where RS-NaCl has the highest sulfate enhancement factor after
462 aging, aqueous reaction results (without NaCl) show a sulfate enhancement trend of
463 WS>CS>RS>IS, suggesting that chloride may take effect in the droplet experiments, especially
464 in RS-NaCl system. Therefore, bulk reaction experiments using ~~rice straw (RS)~~ extracts as an
465 example were performed with 100-200 ppm NaCl additions, where the NaCl to TOC ratio
466 ranged from 100:1 to 200:1 to match the 100:1 to 1000:1 range in droplet experiments, in order
467 to evaluate the effects of chloride on sulfate formation. Interestingly, incorporating NaCl

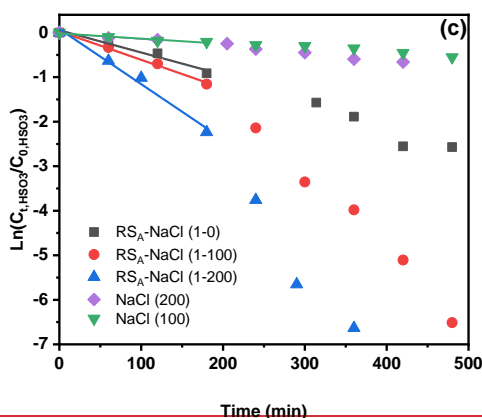
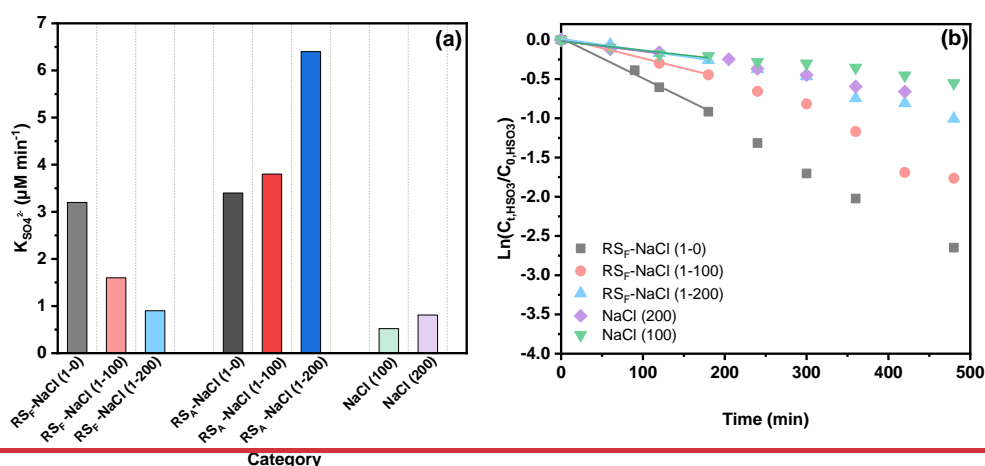
468 yielded contrasting results for RS_F and RS_A (Figure 34). While the addition of NaCl enhanced
469 sulfate formation in RS_A , it showed the opposite trend in RS_F . The nature of the cations and
470 ionic strength may affect the sulfate formation rate; however, previous studies have indicated
471 that their effects are negligible (Zhang and Chan, 2024; Parker and Mitch, 2016). The opposite
472 effect of the NaCl addition on RS_F and RS_A , to some extent, ~~explain~~explains the significantly
473 higher sulfate and SO_2 uptake coefficient enhancement factor for RS-NaCl in Fig. 2. Compared
474 to the RS-based system, NaCl control experiment showed minimum (but non-zero) sulfate
475 formation (Table 1 and Figure 43). On one hand, it ~~confirmed~~supported the findings that
476 chloride participated in the sulfate formation under light but no sulfate formation under dark in
477 bulk reactions, possibly by forming Cl and OH radicals in the presence of air and water (Cao
478 et al., 2024; Tang et al., 2023; Zhang and Chan, 2024). On the other hand, the opposite trend of
479 Cl⁻ effects on RS_F and RS_A reflects its complex interactions with BB extracts under light and
480 air. While direct reaction between S(IV) species and ~~triplet states of photosensitizers~~ ($^3PS^*$)
481 may occur (Wang et al., 2020b), other pathways, i.e., interactions among halide ions,
482 ~~photosensitizers~~ PS and oxygen should also be considered. PS in BB extracts can absorb solar
483 radiation and form ~~triplet state photosensitizer~~ ($^3PS^*$), which can then react with molecular
484 oxygen and form singlet-state oxygen $^1O_2^*$ through energy transfer. $^3PS^*$ can also react with
485 H-donor, typically organic acids (RH, e.g., vanillic acid, succinic acid, azelaic acid, glutaric
486 acid, sorbic acid, salicylic acid, Table S3) through H transfer reactions, and form a ketyl radical
487 ($PSH\bullet$) and an alkyl or phenoxy radical ($R\bullet$). $PSH\bullet$ and $R\bullet$ can then participate in a series of
488 reactions to form $OH\bullet$, $HO_2\bullet$, H_2O_2 and $O_2\bullet^-$. In the presence of a large excess of Cl⁻, Cl⁻ can
489 act as an electron donor, and react with $^3PS^*$, forming a $Cl\bullet$ and a deprotonated ketyl radical
490 ($PS\bullet$) (Jammoul et al., 2009). Further reactions are similar to the abovementioned reactions,
491 including the formation of reactive chlorine species (RCS, i.e., $Cl\bullet$, $Cl_2\bullet^-$ and $ClOH\bullet$) and
492 reactive oxygen species (ROS, i.e., $OH\bullet$, $HO_2\bullet$, H_2O_2 and $O_2\bullet^-$). These RCS and ROS
493 simultaneously contribute to S(IV) oxidation to S(VI) (Zhang and Chan, 2024).

494 Statistical analysis using the Pearson correlation coefficient revealed that the concentrations of
495 CHO, CHON, and CHN species exhibited significant correlations ($|R|>0.5$) with the sulfate
496 formation rate ($p < 0.05$, Figure S9). As PS can be the main CHO species contributing to sulfate
497 formation, N-containing organic compounds (NOCs), i.e., CHN and CHON species, may affect
498 the chloride contribution on sulfate formation rate. Therefore, we selected SyrAld and VL as
499 model CHO (PS), pyrazine (Pyz) as a model CHN, and 4-nitrocatechol (4-NC) as a model
500 CHON to elucidate how potential chemical compounds can alter the effects of chloride on
501 sulfate formation rate by studying the CHO+Cl⁻, CHO+CHN+Cl⁻, and CHO+CHON+Cl⁻
502 systems. For SyrAld and VL, as the $[Cl^-]_0/[PS]_0$ increases, $k_{SO_4^{2-}}$ initially decreases and then
503 increases. The initial decrease of $k_{SO_4^{2-}}$ may be attributed to the quenching of $^3PS^*$ by electron
504 transfer from Cl⁻ or loss of OH radicals by forming ClOH[•] through reaction of $OH\bullet + Cl^-$
505 $\leftrightarrow ClOH\bullet$ (Anastasio and Newberg, 2007). Excessive chloride (e.g. 100 and 200 ppm) may
506 generate Cl and OH radicals through photoexcitation in the presence of air and water and
507 compensate for the loss of $^3PS^*$ or OH radicals. Previous studies have shown controversial
508 influence of halides on the photosensitized oxidation of organic compounds or bisulfite. Parker
509 and Mitch (2016) and Zhang et al. (2023) attributed the significantly higher photodegradation
510 of dienes, thioethers and acetaminophen to the formation of reactive halogen species generated
511 by the reactions of PS and halides. Zhang and Chan (2024) reported that $[Cl^-/PS]_0$ in the range

512 of 1:2 to 4:1 did not lead to significant difference in sulfate formation, possibly due to the
513 insufficient Cl^- concentration in triggering the interplay between PS and Cl^- . The differences
514 between the current results and the aforementioned study might be attributed to the higher $[\text{Cl}^-$
515 $/\text{PS}]_0$ (up to 1:200) which may have been sufficient to initiate the relevant reactions, as well as
516 the difference in photosensitizing capacities of the PS studied (triplet quantum yield of $0.86 \pm$
517 0.05 for 2-IC and 0.21 ± 0.01 for VL) (Felber et al., 2021; 2020). Safiarian et al. (2023) reported
518 that increasing chloride concentrations facilitated anthracene photosensitization by producing
519 high-level reactive oxygen species (ROS). Wang et al. (2023a) found that the effects of chloride
520 on sulfate formation depended on the specific PS: enhancing sulfate production for
521 benzophenone (BP) and 3,4-dimethoxybenzaldehyde (DMB), but decreasing it for 1,4-
522 naphthoquinone.

523 When incorporating CHN species, a 2-3-fold $k_{\text{SO}_4^{2-}}$ was observed, due to the enhanced H
524 transfer by CHN acting as H-bond acceptor (Dou et al., 2015). With the addition of NaCl, the
525 enhanced H-transfer effect by CHN was inhibited, possibly due to the consumption of $^3\text{PS}^*$ by
526 Cl^- . The addition of model CHON species into PS decreased $k_{\text{SO}_4^{2-}}$, due to the consumption of
527 $^3\text{PS}^*$ by CHON species, in agreement with Wang et al. (2023b) who reported increased effective
528 quantum yield of 4-NC when co-photolysis with VL. Further addition of NaCl increased the
529 $k_{\text{SO}_4^{2-}}$, possibly due to the consumption of 4-NC by RCS (Wang et al., 2024b), which, to some
530 extent, reduced the loss of $^3\text{PS}^*$. Generally, the addition of chloride increased $k_{\text{SO}_4^{2-}}$ of PS-
531 CHON but decreased $k_{\text{SO}_4^{2-}}$ of PS-CHN. However, the ambient air is characterized by the
532 presence of tens of thousands of chemical compounds. As a result, the interplay among this
533 diverse array of species may occur in ways that exceed current understanding, necessitating
534 additional research to investigate the interactions between different organic compounds more
535 thoroughly.





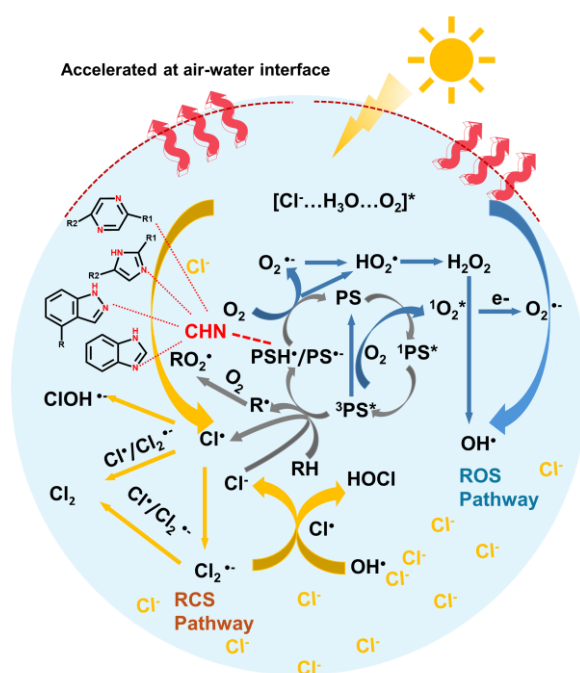
537

538 Figure 34. (a) Sulfate formation rate and (b) (c) bisulfite decay in RS-NaCl aqueous system reactions.
 539 1-0, 1-100, and 1-200 refer to the concentration ratios of TOC_{RS} and NaCl, in which 1, 100, 200
 540 represent 1 ppm, 100 ppm and 200 ppm, respectively.

541 3.4 Proposed mechanism for sulfate formation

542 A conceptual diagram of PS and chloride mediated ROS and RCS production in the oxidation
 543 of S (IV) to S (VI) was shown in Fig. 45. Initially, the photosensitizers-PS (PS, e.g., SyrAld and
 544 VL) absorb solar radiation and produce the singlet state $^1PS^*$, which then undergo a spin
 545 conversion through intersystem crossing, leading to the formation of the triplet state $^3PS^*$. The
 546 $^3PS^*$ can react with molecular oxygen through energy transfer and generate singlet state $^1O_2^*$,
 547 while the $^3PS^*$ returns to ground state. The $^1O_2^*$ can then transform to $O_2^{\bullet-}$ via electron transfer.
 548 The $^3PS^*$ can also react with an H donor (RH, e.g., organic acids, syringol, guaiacol, Table S3),
 549 leading to the formation of alkyl or phenoxy radical ($R\bullet$) and a ketyl radical ($PSH\bullet$). $R\bullet$ can
 550 react with O_2 and form RO_2 radicals while $PSH\bullet$ can transfer an H atom to O_2 and form $HO_2\bullet$,
 551 returning to its ground state PS. Additionally, $^3PS^*$ can react with an electron donor, e.g., Cl,
 552 and form chlorine radicals and $PS^{\bullet-}$. The formed $PS^{\bullet-}$ then reacts with O_2 and form $O_2^{\bullet-}$, which
 553 undergoes a series of reactions and form $HO_2\bullet$, H_2O_2 and $OH\bullet$. The above-mentioned reactions
 554 are the main processes in ROS pathway. Recently, Zhang and Chan(2024) have proposed that
 555 the reactive chlorine species (RCS) would contribute to sulfate formation. Cao et al. (2024)

556 proposed a mechanism of OH and Cl radicals formation by $[\text{Cl}^-\text{H}_3\text{O}^+\text{-O}_2]$ under light irradiation
 557 through an electron transfer process. Our results also demonstrate that the addition of Cl^- will
 558 affect the oxidation process of S(VI) (Figures 34, S10-S12). Combining the above, the RCS
 559 pathway was shown in yellow arrows in Figure 45. The Cl^{\bullet} can be formed in two pathways,
 560 photoexcitation of the $[\text{Cl}^-\text{H}_3\text{O}^+\text{-O}_2]$ complex that generates Cl radicals in deliquescent BB-
 561 NaCl droplets or aqueous BB-NaCl solution (Cao et al., 2024), and PS^* mediated Cl^{\bullet}
 562 formation via electron transfer by Cl^- (Corral Arroyo et al., 2019). The formed Cl^{\bullet} can then
 563 react with each other through radical-radical reactions and produce molecular Cl_2 . The Cl^{\bullet} can
 564 also react with Cl^- or $\text{Cl}_2^{\bullet-}$, forming $\text{Cl}_2^{\bullet-}$ or Cl_2 . Cl^{\bullet} and $\text{Cl}_2^{\bullet-}$ can also react with OH and
 565 form HOCl. $^3\text{PS}^*$ itself can also oxidize the S(IV) (e.g., dissolved SO_2 or bisulfite) to S(VI).
 566 However, significantly lower sulfate formation was found in the presence of N_2 compared to
 567 air condition (Figure 2S3), highlighting the importance of secondary oxidants compared to
 568 direct PS^* oxidation. As a consequence, these reactive species, e.g., $\text{OH}^{\bullet}/\text{HO}_2^{\bullet}/\text{O}_2^{\bullet-}$ and
 569 $\text{Cl}^{\bullet}/\text{Cl}_2^{\bullet-}$ may all participate in the oxidation of S(IV) to S(VI). In addition, the nitrogen-
 570 containing heterocyclic compounds such as pyrazine can act as H-bonding acceptor and
 571 facilitate the H transfer, which then generates more ROS (Dou et al., 2015). In light of the
 572 absence of substantial fluctuations in chloride concentration (Figure S13 and S14, insignificant
 573 chloride concentration change was found even in 10 ppm NaCl addition), it is postulated that
 574 chloride ions may function as a reactive medium rather than as direct reactants. In this proposed
 575 scenario, the Cl radicals and $\text{Cl}_2^{\bullet-}$ intermediates generated during the reaction subsequently
 576 undergo reversion back to Cl^- ions, thereby maintaining a relatively constant Cl^- concentration
 577 throughout the experimental observations. Note that although ROS and RCS pathways both
 578 contribute to the oxidation from S(IV) to S(VI), they may act as competitive relationships due
 579 to the co-consumption of PS^* . Therefore, different Cl effects may occur regarding various
 580 combinations of reactants (Figure 34, promoting effect in RS_A , inhibiting effects on RS_F).



581

582 Figure 45. Conceptual diagram of PS and chloride mediated ROS and RCS production, which

583 participates in the oxidation processes from S(IV) to S(VI)

584 **4 Atmospheric Implication**

585 This study provided laboratory evidence that the ~~photosensitizers-PS~~ in biomass burning
586 extracts can enhance the sulfate formation in NaCl particles, primarily by triggering the
587 formation of secondary oxidants under light and air, with less contribution of direct
588 photosensitization via triplets (evidenced by N₂ atmosphere, Figure S32). The sulfate formation
589 rate of BB_F-NaCl particles were ~10 folds higher than that of IS_F-NaCl, following the trends of CS_F-
590 NaCl>RS_F-NaCl>WS_F-NaCl>IS_F-NaCl. Upon UV exposure, the sulfate formation trends
591 shifted to RS_A-NaCl>CS_A-NaCl>WS_A-NaCl>IS_A-NaCl, which might be explained by the
592 effects of chloride (evidenced by aqueous reactions, Figure 3-4 and Table 1). Interestingly, the
593 incorporation of Cl⁻ into bulk solutions increased the sulfate formation rate in RS_A, while
594 decreased it in RS_F. This seems to be different from our group's previous work where no
595 significant sulfate formation rate was found with the addition of Cl⁻ (Zhang and Chan, 2024).
596 The difference can be explained by the following reasons: 1) differences in PS/Cl⁻, the prior
597 study might use an insufficient PS/Cl⁻ ratio (2:1-1:4) while the current one significantly expands
598 it to 1:200. 2) differences in photosensitizing capacity: the former study used a strong PS, while
599 the current study focused on the real BB (using TOC as metric, with only a small portion of
600 TOC considered as PS). 3) the complexity of the reaction system, the former study focused on
601 mixing two individual species, while in real BB extracts, more complicated reactions may occur.
602 Furthermore, our results using model PS show that although additional model CHN species
603 would increase the sulfate formation by expedited H transfer via acting as H-bond acceptor, the
604 addition of chloride could inhibit the sulfate formation rate, suggesting that the RCS pathway
605 was less efficient in sulfate formation compared to ROS pathway in PS-CHN bulk system
606 (Figure S10 and S11).

607 Previous studies have detected a significant proportion of NOCs, including nitroaromatics
608 (CHON) and reduced nitrogen species (CHN) in biomass burning plumes, wildfires and
609 ambient samples (Zhong et al., 2024; Wang et al., 2017b; Song et al., 2022; Cai et al., 2020).
610 These NOCs are considered as ubiquitous contributors to BrC, and can affect global climate and
611 human health. Moreover, recent research has discovered aerosol pollution in marine
612 background regions, with high levels of NOCs when air masses are transported from wildfires
613 or biomass burning events in nearby (Zhong et al., 2024; Qin et al., 2024). These NOCs,
614 combined with reactive gases, may mix with sea-salt aerosols and impact regional air quality
615 in coastal zones. While our prior study has examined the potential interplay between chloride
616 and PS at limited mixing ratios (up to 4:1 in bulk solution) (Zhang and Chan, 2024), this work
617 expanded the Cl⁻/PS ratio to a broader range (200:1) and systematically identified the
618 interactions among different organics, including PS, NOCs, and chloride, using sulfate
619 formation as a compass. This highlights the importance to study secondary aerosol formation
620 in mixed experimental system under air pollution complex. Our work suggests that in coastal
621 regions heavily influenced by anthropogenic emissions like biomass burning, especially those
622 near the rice-growing regions or affected by transported wildfire smoke, such as Guangdong,
623 Fujian and Taiwan, the transported BB plumes together with the high RH (Cheung et al., 2015)
624 and abundant reactive gases, would play an inevitable role in sulfate and potentially secondary

625 organic aerosol formation.

626 **Data availability**

627 Datasets are available upon request to the corresponding author, Chak K. Chan
628 (chak.chan@kaust.edu.sa).

629 **Author contributions**

630 RT and CC conceptualized and designed the study. YQ and YC collected the samples. RT
631 performed the experiments, data analysis and wrote the draft. JM provided assistance in data
632 processing. All the authors reviewed, edited and contributed to the scientific discussions.

633 **Competing interests**

634 The authors declare no conflicts of interest.

635 **Acknowledgments**

636 We gratefully acknowledge the support from the Hong Kong Research Grants Council (No.
637 11314222), the National Natural Science Foundation of China (42107115), and the Natural
638 Science Foundation of Shandong Province, China (ZR2021QD111). The authors also thank the
639 University Research Facility in Chemical and Environmental Analysis (UCEA) at The Hong
640 Kong Polytechnic University for the use of its UHPLC-HESI-Orbitrap Mass Spectrometer and
641 Dr Sirius Tse and Dr Chi Hang Chow for assistance with sample analyses.

642 **References**

- 643 Alexander, B., Allman, D. J., Amos, H. M., Fairlie, T. D., Dachs, J., Hegg, D. A., and Sletten, R. S.:
644 Isotopic constraints on the formation pathways of sulfate aerosol in the marine boundary layer of the
645 subtropical northeast Atlantic Ocean, *Journal of Geophysical Research: Atmospheres*, 117,
646 <https://doi.org/10.1029/2011JD016773>, 2012.
- 647 Anastasio, C. and Newberg, J. T.: Sources and sinks of hydroxyl radical in sea-salt particles, *Journal of*
648 *Geophysical Research: Atmospheres*, 112, 2007.
- 649 Andreae, M. O.: Emission of trace gases and aerosols from biomass burning – an updated assessment,
650 *Atmos. Chem. Phys.*, 19, 8523-8546, 10.5194/acp-19-8523-2019, 2019.
- 651 Bond, T. C., Doherty, S. J., Fahey, D. W., Forster, P. M., Berntsen, T., DeAngelo, B. J., Flanner, M. G.,
652 Ghan, S., Kärcher, B., Koch, D., Kinne, S., Kondo, Y., Quinn, P. K., Sarofim, M. C., Schultz, M. G.,
653 Schulz, M., Venkataraman, C., Zhang, H., Zhang, S., Bellouin, N., Guttikunda, S. K., Hopke, P. K.,
654 Jacobson, M. Z., Kaiser, J. W., Klimont, Z., Lohmann, U., Schwarz, J. P., Shindell, D., Storelvmo, T.,
655 Warren, S. G., and Zender, C. S.: Bounding the role of black carbon in the climate system: A scientific
656 assessment, *Journal of Geophysical Research: Atmospheres*, 118, 5380-5552,
657 <https://doi.org/10.1002/jgrd.50171>, 2013.
- 658 Cai, J., Zeng, X., Zhi, G., Gligorovski, S., Sheng, G., Yu, Z., Wang, X., and Peng, P.: Molecular
659 composition and photochemical evolution of water-soluble organic carbon (WSOC) extracted from field
660 biomass burning aerosols using high-resolution mass spectrometry, *Atmos. Chem. Phys.*, 20, 6115-6128,
661 10.5194/acp-20-6115-2020, 2020.
- 662 Calderon-Arrieta, D., Morales, A. C., Hettiyadura, A. P. S., Estock, T. M., Li, C., Rudich, Y., and Laskin,

663 A.: Enhanced Light Absorption and Elevated Viscosity of Atmospheric Brown Carbon through
664 Evaporation of Volatile Components, *Environmental Science & Technology*, 58, 7493-7504,
665 10.1021/acs.est.3c10184, 2024.

666 Cao, Y., Liu, J., Ma, Q., Zhang, C., Zhang, P., Chen, T., Wang, Y., Chu, B., Zhang, X., Francisco, J. S.,
667 and He, H.: Photoactivation of Chlorine and Its Catalytic Role in the Formation of Sulfate Aerosols,
668 *Journal of the American Chemical Society*, 146, 1467-1475, 10.1021/jacs.3c10840, 2024.

669 Charlson, R. J., Schwartz, S. E., Hales, J. M., Cess, R. D., Coakley, J. A., Hansen, J. E., and Hofmann,
670 D. J.: Climate Forcing by Anthropogenic Aerosols, *Science*, 255, 423-430,
671 doi:10.1126/science.255.5043.423, 1992.

672 Chen, J., Li, C., Ristovski, Z., Milic, A., Gu, Y., Islam, M. S., Wang, S., Hao, J., Zhang, H., He, C., Guo,
673 H., Fu, H., Miljevic, B., Morawska, L., Thai, P., Lam, Y. F., Pereira, G., Ding, A., Huang, X., and Dumka,
674 U. C.: A review of biomass burning: Emissions and impacts on air quality, health and climate in China,
675 *Science of The Total Environment*, 579, 1000-1034, <https://doi.org/10.1016/j.scitotenv.2016.11.025>,
676 2017.

677 Chen, Y., Zheng, P., Wang, Z., Pu, W., Tan, Y., Yu, C., Xia, M., Wang, W., Guo, J., Huang, D., Yan, C.,
678 Nie, W., Ling, Z., Chen, Q., Lee, S., and Wang, T.: Secondary Formation and Impacts of Gaseous Nitro-
679 Phenolic Compounds in the Continental Outflow Observed at a Background Site in South China,
680 *Environmental Science & Technology*, 56, 6933-6943, 10.1021/acs.est.1c04596, 2022.

681 Cheng, S.-B., Zhou, C.-H., Yin, H.-M., Sun, J.-L., and Han, K.-L.: OH produced from o-nitrophenol
682 photolysis: A combined experimental and theoretical investigation, *The Journal of chemical physics*, 130,
683 2009.

684 Cheung, H. H., Yeung, M. C., Li, Y. J., Lee, B. P., and Chan, C. K.: Relative humidity-dependent HTDMA
685 measurements of ambient aerosols at the HKUST supersite in Hong Kong, China, *Aerosol Science and*
686 *Technology*, 49, 643-654, 2015.

687 Chi, J. W., Li, W. J., Zhang, D. Z., Zhang, J. C., Lin, Y. T., Shen, X. J., Sun, J. Y., Chen, J. M., Zhang, X.
688 Y., Zhang, Y. M., and Wang, W. X.: Sea salt aerosols as a reactive surface for inorganic and organic acidic
689 gases in the Arctic troposphere, *Atmos. Chem. Phys.*, 15, 11341-11353, 10.5194/acp-15-11341-2015,
690 2015.

691 Corral Arroyo, P., Aellig, R., Alpert, P. A., Volkamer, R., and Ammann, M.: Halogen activation and
692 radical cycling initiated by imidazole-2-carboxaldehyde photochemistry, *Atmospheric Chemistry and*
693 *Physics*, 19, 10817-10828, 2019.

694 Donaldson, D. J., Kroll, J. A., and Vaida, V.: Gas-phase hydrolysis of triplet SO₂: A possible direct route
695 to atmospheric acid formation, *Scientific Reports*, 6, 30000, 10.1038/srep30000, 2016.

696 Dou, J., Lin, P., Kuang, B.-Y., and Yu, J. Z.: Reactive Oxygen Species Production Mediated by Humic-
697 like Substances in Atmospheric Aerosols: Enhancement Effects by Pyridine, Imidazole, and Their
698 Derivatives, *Environmental Science & Technology*, 49, 6457-6465, 10.1021/es5059378, 2015.

699 Fang, Z., Deng, W., Zhang, Y., Ding, X., Tang, M., Liu, T., Hu, Q., Zhu, M., Wang, Z., Yang, W., Huang,
700 Z., Song, W., Bi, X., Chen, J., Sun, Y., George, C., and Wang, X.: Open burning of rice, corn and wheat
701 straws: primary emissions, photochemical aging, and secondary organic aerosol formation, *Atmos. Chem.*
702 *Phys.*, 17, 14821-14839, 10.5194/acp-17-14821-2017, 2017.

703 Felber, T., Schaefer, T., and Herrmann, H.: Five-Membered Heterocycles as Potential Photosensitizers in
704 the Tropospheric Aqueous Phase: Photophysical Properties of Imidazole-2-carboxaldehyde, 2-
705 Furaldehyde, and 2-Acetylfuran, *The Journal of Physical Chemistry A*, 124, 10029-10039,
706 10.1021/acs.jpca.0c07028, 2020.

707 Felber, T., Schaefer, T., He, L., and Herrmann, H.: Aromatic Carbonyl and Nitro Compounds as
708 Photosensitizers and Their Photophysical Properties in the Tropospheric Aqueous Phase, *The Journal of*
709 *Physical Chemistry A*, 125, 5078-5095, 10.1021/acs.jpca.1c03503, 2021.

710 Fu, H., Ciuraru, R., Dupart, Y., Passananti, M., Tinel, L., Rossignol, S., Perrier, S., Donaldson, D. J.,
711 Chen, J., and George, C.: Photosensitized Production of Atmospherically Reactive Organic Compounds
712 at the Air/Aqueous Interface, *Journal of the American Chemical Society*, 137, 8348-8351,
713 10.1021/jacs.5b04051, 2015.

714 Fushimi, A., Saitoh, K., Hayashi, K., Ono, K., Fujitani, Y., Villalobos, A. M., Shelton, B. R., Takami, A.,
715 Tanabe, K., and Schauer, J. J.: Chemical characterization and oxidative potential of particles emitted
716 from open burning of cereal straws and rice husk under flaming and smoldering conditions, *Atmospheric*
717 *Environment*, 163, 118-127, <https://doi.org/10.1016/j.atmosenv.2017.05.037>, 2017.

718 Fuzzi, S., Baltensperger, U., Carslaw, K., Decesari, S., Denier van der Gon, H., Facchini, M. C., Fowler,
719 D., Koren, I., Langford, B., Lohmann, U., Nemitz, E., Pandis, S., Riipinen, I., Rudich, Y., Schaap, M.,
720 Slowik, J. G., Spracklen, D. V., Vignati, E., Wild, M., Williams, M., and Gilardoni, S.: Particulate matter,
721 air quality and climate: lessons learned and future needs, *Atmos. Chem. Phys.*, 15, 8217-8299,
722 10.5194/acp-15-8217-2015, 2015.

723 Gantt, B. and Meskhidze, N.: The physical and chemical characteristics of marine primary organic
724 aerosol: a review, *Atmos. Chem. Phys.*, 13, 3979-3996, 10.5194/acp-13-3979-2013, 2013.

725 Gemayel, R., Emmelin, C., Perrier, S., Tomaz, S., Baboosian, V., Fishman, D., Nizkorodov, S., Dumas,
726 S., and George, C.: Quenching of ketone triplet excited states by atmospheric halides, *Environmental*
727 *Science: Atmospheres*, 1, 31-44, 2021.

728 Gen, M., Zhang, R., Huang, D. D., Li, Y., and Chan, C. K.: Heterogeneous Oxidation of SO₂ in Sulfate
729 Production during Nitrate Photolysis at 300 nm: Effect of pH, Relative Humidity, Irradiation Intensity,
730 and the Presence of Organic Compounds, *Environmental Science & Technology*, 53, 8757-8766,
731 10.1021/acs.est.9b01623, 2019a.

732 Gen, M., Zhang, R., Huang, D. D., Li, Y., and Chan, C. K.: Heterogeneous SO₂ Oxidation in Sulfate
733 Formation by Photolysis of Particulate Nitrate, *Environmental Science & Technology Letters*, 6, 86-91,
734 10.1021/acs.estlett.8b00681, 2019b.

735 Gómez Alvarez, E., Wortham, H., Strekowski, R., Zetzsch, C., and Gligorovski, S.: Atmospheric
736 Photosensitized Heterogeneous and Multiphase Reactions: From Outdoors to Indoors, *Environmental*
737 *Science & Technology*, 46, 1955-1963, 10.1021/es2019675, 2012.

738 Gong, C., Yuan, X., Xing, D., Zhang, D., Martins-Costa, M. T. C., Anglada, J. M., Ruiz-López, M. F.,
739 Francisco, J. S., and Zhang, X.: Fast Sulfate Formation Initiated by the Spin-Forbidden Excitation of
740 SO₂ at the Air–Water Interface, *Journal of the American Chemical Society*, 144, 22302-22308,
741 10.1021/jacs.2c10830, 2022.

742 Guo, S. and Li, H.: Photolysis of nitrophenols in gas phase and aqueous environment: a potential daytime
743 source for atmospheric nitrous acid (HONO), *Environmental Science: Atmospheres*, 3, 143-155, 2023.

744 Hu, W., Zhou, H., Chen, W., Ye, Y., Pan, T., Wang, Y., Song, W., Zhang, H., Deng, W., Zhu, M., Wang,
745 C., Wu, C., Ye, C., Wang, Z., Yuan, B., Huang, S., Shao, M., Peng, Z., Day, D. A., Campuzano-Jost, P.,
746 Lambe, A. T., Worsnop, D. R., Jimenez, J. L., and Wang, X.: Oxidation Flow Reactor Results in a Chinese
747 Megacity Emphasize the Important Contribution of S/IVOCs to Ambient SOA Formation,
748 *Environmental Science & Technology*, 56, 6880-6893, 10.1021/acs.est.1c03155, 2022.

749 Huang, G., Wang, S., Chang, X., Cai, S., Zhu, L., Li, Q., and Jiang, J.: Emission factors and chemical
750 profile of I/SVOCs emitted from household biomass stove in China, *Science of The Total Environment*,

751 842, 156940, <https://doi.org/10.1016/j.scitotenv.2022.156940>, 2022a.

752 Huang, R.-J., Yang, L., Shen, J., Yuan, W., Gong, Y., Ni, H., Duan, J., Yan, J., Huang, H., You, Q., and
753 Li, Y. J.: Chromophoric Fingerprinting of Brown Carbon from Residential Biomass Burning,
754 Environmental Science & Technology Letters, 9, 102-111, 10.1021/acs.estlett.1c00837, 2022b.

755 Huang, S., Wu, Z., Poulain, L., van Pinxteren, M., Merkel, M., Assmann, D., Herrmann, H., and
756 Wiedensohler, A.: Source apportionment of the organic aerosol over the Atlantic Ocean from
757 53° N to 53° S: significant contributions from marine emissions and long-range transport,
758 Atmos. Chem. Phys., 18, 18043-18062, 10.5194/acp-18-18043-2018, 2018.

759 Hung, H.-M. and Hoffmann, M. R.: Oxidation of Gas-Phase SO₂ on the Surfaces of Acidic Microdroplets:
760 Implications for Sulfate and Sulfate Radical Anion Formation in the Atmospheric Liquid Phase,
761 Environmental Science & Technology, 49, 13768-13776, 10.1021/acs.est.5b01658, 2015.

762 Jammoul, A., Dumas, S., D'Anna, B., and George, C.: Photoinduced oxidation of sea salt halides by
763 aromatic ketones: a source of halogenated radicals, Atmos. Chem. Phys., 9, 4229-4237, 10.5194/acp-9-
764 4229-2009, 2009.

765 Jiang, H., Carena, L., He, Y., Wang, Y., Zhou, W., Yang, L., Luan, T., Li, X., Brigante, M., Vione, D., and
766 Gligorovski, S.: Photosensitized Degradation of DMSO Initiated by PAHs at the Air-Water Interface, as
767 an Alternative Source of Organic Sulfur Compounds to the Atmosphere, Journal of Geophysical Research:
768 Atmospheres, 126, e2021JD035346, <https://doi.org/10.1029/2021JD035346>, 2021.

769 Jones, M. W., Abatzoglou, J. T., Veraverbeke, S., Andela, N., Lasslop, G., Forkel, M., Smith, A. J. P.,
770 Burton, C., Betts, R. A., van der Werf, G. R., Sitch, S., Canadell, J. G., Santín, C., Kolden, C., Doerr, S.
771 H., and Le Quéré, C.: Global and Regional Trends and Drivers of Fire Under Climate Change, Reviews
772 of Geophysics, 60, e2020RG000726, <https://doi.org/10.1029/2020RG000726>, 2022.

773 Jungwirth, P. and Tobias, D. J.: Chloride Anion on Aqueous Clusters, at the Air–Water Interface, and in
774 Liquid Water: Solvent Effects on Cl⁻ Polarizability, The Journal of Physical Chemistry A, 106, 379-383,
775 10.1021/jp012059d, 2002.

776 Jungwirth, P. and Tobias, D. J.: Specific Ion Effects at the Air/Water Interface, Chemical Reviews, 106,
777 1259-1281, 10.1021/cr0403741, 2006.

778 Kalogridis, A. C., Popovicheva, O. B., Engling, G., Diapouli, E., Kawamura, K., Tachibana, E., Ono, K.,
779 Kozlov, V. S., and Eleftheriadis, K.: Smoke aerosol chemistry and aging of Siberian biomass burning
780 emissions in a large aerosol chamber, Atmospheric Environment, 185, 15-28,
781 <https://doi.org/10.1016/j.atmosenv.2018.04.033>, 2018.

782 Kim, Y. H., Warren, S. H., Krantz, Q. T., King, C., Jaskot, R., Preston, W. T., George, B. J., Hays, M. D.,
783 Landis, M. S., and Higuchi, M.: Mutagenicity and lung toxicity of smoldering vs. flaming emissions
784 from various biomass fuels: implications for health effects from wildland fires, Environmental health
785 perspectives, 126, 017011, 2018.

786 Kim, Y. H., Warren, S. H., Kooter, I., Williams, W. C., George, I. J., Vance, S. A., Hays, M. D., Higuchi,
787 M. A., Gavett, S. H., DeMarini, D. M., Jaspers, I., and Gilmour, M. I.: Chemistry, lung toxicity and
788 mutagenicity of burn pit smoke-related particulate matter, Particle and Fibre Toxicology, 18, 45,
789 10.1186/s12989-021-00435-w, 2021.

790 Kipp, B. H., Faraj, C., Li, G., and Njus, D.: Imidazole facilitates electron transfer from organic reductants,
791 Bioelectrochemistry, 64, 7-13, <https://doi.org/10.1016/j.bioelechem.2003.12.010>, 2004.

792 Koch, B. P. and Dittmar, T.: From mass to structure: An aromaticity index for high-resolution mass data
793 of natural organic matter, Rapid communications in mass spectrometry, 20, 926-932, 2006.

794 Laskin, A., Laskin, J., and Nizkorodov, S. A.: Chemistry of Atmospheric Brown Carbon, Chemical

795 Reviews, 115, 4335-4382, 10.1021/cr5006167, 2015.

796 Laskin, A., Smith, J. S., and Laskin, J.: Molecular Characterization of Nitrogen-Containing Organic
797 Compounds in Biomass Burning Aerosols Using High-Resolution Mass Spectrometry, *Environmental*
798 *Science & Technology*, 43, 3764-3771, 10.1021/es803456n, 2009.

799 Liang, Z., Li, Y., Go, B. R., and Chan, C. K.: Complexities of Photosensitization in Atmospheric Particles,
800 *ACS ES&T Air*, 10.1021/acsestair.4c00112, 2024.

801 Liang, Z., Zhou, L., Infante Cuevas, R. A., Li, X., Cheng, C., Li, M., Tang, R., Zhang, R., Lee, P. K. H.,
802 Lai, A. C. K., and Chan, C. K.: Sulfate Formation in Incense Burning Particles: A Single-Particle Mass
803 Spectrometric Study, *Environmental Science & Technology Letters*, 9, 718-725,
804 10.1021/acs.estlett.2c00492, 2022.

805 Lin, P., Rincon, A. G., Kalberer, M., and Yu, J. Z.: Elemental Composition of HULIS in the Pearl River
806 Delta Region, China: Results Inferred from Positive and Negative Electrospray High Resolution Mass
807 Spectrometric Data, *Environmental Science & Technology*, 46, 7454-7462, 10.1021/es300285d, 2012.

808 Lin, P., Fleming, L. T., Nizkorodov, S. A., Laskin, J., and Laskin, A.: Comprehensive Molecular
809 Characterization of Atmospheric Brown Carbon by High Resolution Mass Spectrometry with
810 Electrospray and Atmospheric Pressure Photoionization, *Analytical Chemistry*, 90, 12493-12502,
811 10.1021/acs.analchem.8b02177, 2018.

812 Lin, P., Aiona, P. K., Li, Y., Shiraiwa, M., Laskin, J., Nizkorodov, S. A., and Laskin, A.: Molecular
813 Characterization of Brown Carbon in Biomass Burning Aerosol Particles, *Environmental Science &*
814 *Technology*, 50, 11815-11824, 10.1021/acs.est.6b03024, 2016.

815 Liu, D., Zhang, Y., Zhong, S., Chen, S., Xie, Q., Zhang, D., Zhang, Q., Hu, W., Deng, J., Wu, L., Ma, C.,
816 Tong, H., and Fu, P.: Large differences of highly oxygenated organic molecules (HOMs) and low-volatile
817 species in secondary organic aerosols (SOAs) formed from ozonolysis of β -pinene and limonene, *Atmos.*
818 *Chem. Phys.*, 23, 8383-8402, 10.5194/acp-23-8383-2023, 2023a.

819 Liu, H., Pei, X., Zhang, F., Song, Y., Kuang, B., Xu, Z., and Wang, Z.: Relative Humidity Dependence
820 of Growth Factor and Real Refractive Index for Sea Salt/Malonic Acid Internally Mixed Aerosols,
821 *Journal of Geophysical Research: Atmospheres*, 128, e2022JD037579,
822 <https://doi.org/10.1029/2022JD037579>, 2023b.

823 Liu, T. and Abbatt, J. P. D.: Oxidation of sulfur dioxide by nitrogen dioxide accelerated at the interface
824 of deliquesced aerosol particles, *Nature Chemistry*, 13, 1173-1177, 10.1038/s41557-021-00777-0, 2021.

825 Liu, T., Clegg, S. L., and Abbatt, J. P.: Fast oxidation of sulfur dioxide by hydrogen peroxide in
826 deliquesced aerosol particles, *Proceedings of the National Academy of Sciences*, 117, 1354-1359, 2020.

827 Mabato, B. R. G., Li, Y. J., Huang, D. D., Wang, Y., and Chan, C. K.: Comparison of aqueous secondary
828 organic aerosol (aqSOA) product distributions from guaiacol oxidation by non-phenolic and phenolic
829 methoxybenzaldehydes as photosensitizers in the absence and presence of ammonium nitrate, *Atmos.*
830 *Chem. Phys.*, 23, 2859-2875, 10.5194/acp-23-2859-2023, 2023.

831 Mabato, B. R. G., Lyu, Y., Ji, Y., Li, Y. J., Huang, D. D., Li, X., Nah, T., Lam, C. H., and Chan, C. K.:
832 Aqueous secondary organic aerosol formation from the direct photosensitized oxidation of vanillin in the
833 absence and presence of ammonium nitrate, *Atmos. Chem. Phys.*, 22, 273-293, 10.5194/acp-22-273-
834 2022, 2022.

835 Mao, J., Ren, X., Brune, W. H., Olson, J. R., Crawford, J. H., Fried, A., Huey, L. G., Cohen, R. C., Heikes,
836 B., Singh, H. B., Blake, D. R., Sachse, G. W., Diskin, G. S., Hall, S. R., and Shetter, R. E.: Airborne
837 measurement of OH reactivity during INTEX-B, *Atmos. Chem. Phys.*, 9, 163-173, 10.5194/acp-9-163-
838 2009, 2009.

839 Mauldin III, R. L., Berndt, T., Sipilä, M., Paasonen, P., Petäjä, T., Kim, S., Kurtén, T., Stratmann, F.,
840 Kerminen, V. M., and Kulmala, M.: A new atmospherically relevant oxidant of sulphur dioxide, *Nature*,
841 488, 193-196, 10.1038/nature11278, 2012.

842 Mohr, C., Lopez-Hilfiker, F. D., Zotter, P., Prévôt, A. S. H., Xu, L., Ng, N. L., Herndon, S. C., Williams,
843 L. R., Franklin, J. P., Zahniser, M. S., Worsnop, D. R., Knighton, W. B., Aiken, A. C., Gorkowski, K. J.,
844 Dubey, M. K., Allan, J. D., and Thornton, J. A.: Contribution of Nitrated Phenols to Wood Burning Brown
845 Carbon Light Absorption in Detling, United Kingdom during Winter Time, *Environmental Science &*
846 *Technology*, 47, 6316-6324, 10.1021/es400683v, 2013.

847 Nel, A.: Air Pollution-Related Illness: Effects of Particles, *Science*, 308, 804-806,
848 doi:10.1126/science.1108752, 2005.

849 Parker, K. M. and Mitch, W. A.: Halogen radicals contribute to photooxidation in coastal and estuarine
850 waters, *Proceedings of the National Academy of Sciences*, 113, 5868-5873, 2016.

851 Peng, Z. and Jimenez, J. L.: Radical chemistry in oxidation flow reactors for atmospheric chemistry
852 research, *Chemical Society Reviews*, 49, 2570-2616, 2020.

853 Pozzoli, L., Gilardoni, S., Perrone, M. G., de Gennaro, G., de Rienzo, M., and Vione, D.: POLYCYCLIC
854 AROMATIC HYDROCARBONS IN THE ATMOSPHERE: MONITORING, SOURCES, SINKS AND
855 FATE. I: MONITORING AND SOURCES, *Annali di Chimica*, 94, 17-33,
856 <https://doi.org/10.1002/adic.200490002>, 2004.

857 Qin, Y., Wang, H., Wang, Y., Lu, X., Tang, H., Zhang, J., Li, L., and Fan, S.: Wildfires in Southeast Asia
858 pollute the atmosphere in the northern South China Sea, *Science Bulletin*, 69, 1011-1015,
859 <https://doi.org/10.1016/j.scib.2024.02.026>, 2024.

860 Qiu, Y., Wu, X., Zhang, Y., Xu, L., Hong, Y., Chen, J., Chen, X., and Deng, J.: Aerosol light absorption
861 in a coastal city in Southeast China: Temporal variations and implications for brown carbon, *Journal of*
862 *Environmental Sciences*, 80, 257-266, <https://doi.org/10.1016/j.jes.2019.01.002>, 2019.

863 Rowe, J. P., Lambe, A. T., and Brune, W. H.: Technical Note: Effect of varying the $\lambda = 185$ and
864 254 nm photon flux ratio on radical generation in oxidation flow reactors, *Atmos. Chem. Phys.*,
865 20, 13417-13424, 10.5194/acp-20-13417-2020, 2020.

866 Ruiz-Lopez, M. F., Francisco, J. S., Martins-Costa, M. T. C., and Anglada, J. M.: Molecular reactions at
867 aqueous interfaces, *Nature Reviews Chemistry*, 4, 459-475, 10.1038/s41570-020-0203-2, 2020.

868 Safarian, M. S., Ugboya, A., Khan, I., Marichev, K. O., and Grant, K. B.: New Insights into the
869 Phototoxicity of Anthracene-Based Chromophores: The Chloride Salt Effect, *Chemical Research in*
870 *Toxicology*, 36, 1002-1020, 10.1021/acs.chemrestox.2c00235, 2023.

871 Salvador, C. M. G., Tang, R., Priestley, M., Li, L. J., Tsiligiannis, E., Le Breton, M., Zhu, W., Zeng, L.,
872 Wang, H., and Yu, Y.: Ambient nitro-aromatic compounds—biomass burning versus secondary formation
873 in rural China, *Atmospheric Chemistry and Physics Discussions*, 2020, 1-36, 2020.

874 Sangwan, M. and Zhu, L.: Absorption cross sections of 2-nitrophenol in the 295–400 nm region and
875 photolysis of 2-nitrophenol at 308 and 351 nm, *The Journal of Physical Chemistry A*, 120, 9958-9967,
876 2016.

877 Sangwan, M. and Zhu, L.: Role of Methyl-2-nitrophenol Photolysis as a Potential Source of OH Radicals
878 in the Polluted Atmosphere: Implications from Laboratory Investigation, *The Journal of Physical*
879 *Chemistry A*, 122, 1861-1872, 10.1021/acs.jpca.7b11235, 2018.

880 Schill, G. P., Froyd, K. D., Bian, H., Kupc, A., Williamson, C., Brock, C. A., Ray, E., Hornbrook, R. S.,
881 Hills, A. J., Apel, E. C., Chin, M., Colarco, P. R., and Murphy, D. M.: Widespread biomass burning smoke
882 throughout the remote troposphere, *Nature Geoscience*, 13, 422-427, 10.1038/s41561-020-0586-1, 2020.

883 Seinfeld, J. H. and Pandis, S. N.: Atmospheric chemistry and physics: from air pollution to climate
884 change, John Wiley & Sons 2016.

885 Song, J., Li, M., Zou, C., Cao, T., Fan, X., Jiang, B., Yu, Z., Jia, W., and Peng, P. a.: Molecular
886 Characterization of Nitrogen-Containing Compounds in Humic-like Substances Emitted from Biomass
887 Burning and Coal Combustion, *Environmental Science & Technology*, 56, 119-130,
888 10.1021/acs.est.1c04451, 2022.

889 Song, K., Tang, R., Li, A., Wan, Z., Zhang, Y., Gong, Y., Lv, D., Lu, S., Tan, Y., Yan, S., Yan, S., Zhang,
890 J., Fan, B., Chan, C. K., and Guo, S.: Particulate organic emissions from incense-burning smoke:
891 Chemical compositions and emission characteristics, *Science of The Total Environment*, 897, 165319,
892 <https://doi.org/10.1016/j.scitotenv.2023.165319>, 2023.

893 Stockwell, W. R. and Calvert, J. G.: The mechanism of the HO-SO₂ reaction, *Atmospheric Environment*
894 (1967), 17, 2231-2235, [https://doi.org/10.1016/0004-6981\(83\)90220-2](https://doi.org/10.1016/0004-6981(83)90220-2), 1983.

895 Tang, R., Zhang, R., Ma, J., Song, K., Mabato, B. R. G., Cuevas, R. A. I., Zhou, L., Liang, Z., Vogel, A.
896 L., Guo, S., and Chan, C. K.: Sulfate Formation by Photosensitization in Mixed Incense Burning–Sodium
897 Chloride Particles: Effects of RH, Light Intensity, and Aerosol Aging, *Environmental Science &*
898 *Technology*, 57, 10295-10307, 10.1021/acs.est.3c02225, 2023.

899 Tinel, L., Rossignol, S., Bianco, A., Passananti, M., Perrier, S., Wang, X., Brigante, M., Donaldson, D.
900 J., and George, C.: Mechanistic Insights on the Photosensitized Chemistry of a Fatty Acid at the
901 Air/Water Interface, *Environmental Science & Technology*, 50, 11041-11048, 10.1021/acs.est.6b03165,
902 2016.

903 Ting, Y., Mitchell, E. J. S., Allan, J. D., Liu, D., Spracklen, D. V., Williams, A., Jones, J. M., Lea-Langton,
904 A. R., McFiggans, G., and Coe, H.: Mixing State of Carbonaceous Aerosols of Primary Emissions from
905 “Improved” African Cookstoves, *Environmental Science & Technology*, 52, 10134-10143,
906 10.1021/acs.est.8b00456, 2018.

907 Tkacik, D. S., Lambe, A. T., Jathar, S., Li, X., Presto, A. A., Zhao, Y., Blake, D., Meinardi, S., Jayne, J.
908 T., Croteau, P. L., and Robinson, A. L.: Secondary Organic Aerosol Formation from in-Use Motor Vehicle
909 Emissions Using a Potential Aerosol Mass Reactor, *Environmental Science & Technology*, 48, 11235-
910 11242, 10.1021/es502239v, 2014.

911 van Pinxteren, M., Fiedler, B., van Pinxteren, D., Iinuma, Y., Körtzinger, A., and Herrmann, H.: Chemical
912 characterization of sub-micrometer aerosol particles in the tropical Atlantic Ocean: marine and biomass
913 burning influences, *Journal of Atmospheric Chemistry*, 72, 105-125, 10.1007/s10874-015-9307-3, 2015.

914 Wang, J., Li, J., Ye, J., Zhao, J., Wu, Y., Hu, J., Liu, D., Nie, D., Shen, F., and Huang, X.: Fast sulfate
915 formation from oxidation of SO₂ by NO₂ and HONO observed in Beijing haze, *Nature Communications*,
916 11, 2844, 2020a.

917 Wang, K., Zhang, Y., Tong, H., Han, J., Fu, P., Huang, R.-J., Zhang, H., and Hoffmann, T.: Molecular-
918 Level Insights into the Relationship between Volatility of Organic Aerosol Constituents and PM_{2.5} Air
919 Pollution Levels: A Study with Ultrahigh-Resolution Mass Spectrometry, *Environmental Science &*
920 *Technology*, 58, 7947-7957, 10.1021/acs.est.3c10662, 2024a.

921 Wang, N., Zhou, D., Liu, H., Tu, Y., Ma, Y., and Li, Y.: Triplet-Excited Dissolved Organic Matter
922 Efficiently Promoted Atmospheric Sulfate Production: Kinetics and Mechanisms, *Separations*, 10, 335,
923 2023a.

924 Wang, S., Liu, T., Jang, J., Abbatt, J. P. D., and Chan, A. W. H.: Heterogeneous interactions between SO₂
925 and organic peroxides in submicron aerosol, *Atmos. Chem. Phys.*, 21, 6647-6661, 10.5194/acp-21-6647-
926 2021, 2021a.

927 Wang, T., Deng, L., Tan, C., Hu, J., and Singh, R. P.: Comparative analysis of chlorinated disinfection
928 byproducts formation from 4-nitrophenol and 2-amino-4-nitrophenol during UV/post-chlorination,
929 Science of The Total Environment, 927, 172200, <https://doi.org/10.1016/j.scitotenv.2024.172200>, 2024b.

930 Wang, W., Liu, Y., Wang, T., Ge, Q., Li, K., Liu, J., You, W., Wang, L., Xie, L., Fu, H., Chen, J., and
931 Zhang, L.: Significantly Accelerated Photosensitized Formation of Atmospheric Sulfate at the Air–Water
932 Interface of Microdroplets, Journal of the American Chemical Society, 146, 6580-6590,
933 10.1021/jacs.3c11892, 2024c.

934 Wang, W., Liu, M., Wang, T., Song, Y., Zhou, L., Cao, J., Hu, J., Tang, G., Chen, Z., Li, Z., Xu, Z., Peng,
935 C., Lian, C., Chen, Y., Pan, Y., Zhang, Y., Sun, Y., Li, W., Zhu, T., Tian, H., and Ge, M.: Sulfate formation
936 is dominated by manganese-catalyzed oxidation of SO₂ on aerosol surfaces during haze events, Nature
937 Communications, 12, 1993, 10.1038/s41467-021-22091-6, 2021b.

938 Wang, X., Gu, R., Wang, L., Xu, W., Zhang, Y., Chen, B., Li, W., Xue, L., Chen, J., and Wang, W.:
939 Emissions of fine particulate nitrated phenols from the burning of five common types of biomass,
940 Environmental Pollution, 230, 405-412, <https://doi.org/10.1016/j.envpol.2017.06.072>, 2017a.

941 Wang, X., Gemayel, R., Hayeck, N., Perrier, S., Charbonnel, N., Xu, C., Chen, H., Zhu, C., Zhang, L.,
942 Wang, L., Nizkorodov, S. A., Wang, X., Wang, Z., Wang, T., Mellouki, A., Riva, M., Chen, J., and George,
943 C.: Atmospheric Photosensitization: A New Pathway for Sulfate Formation, Environmental Science &
944 Technology, 54, 3114-3120, 10.1021/acs.est.9b06347, 2020b.

945 Wang, Y., Hu, M., Xu, N., Qin, Y., Wu, Z., Zeng, L., Huang, X., and He, L.: Chemical composition and
946 light absorption of carbonaceous aerosols emitted from crop residue burning: influence of combustion
947 efficiency, Atmos. Chem. Phys., 20, 13721-13734, 10.5194/acp-20-13721-2020, 2020c.

948 Wang, Y., Qiu, T., Zhang, C., Hao, T., Mabato, B. R. G., Zhang, R., Gen, M., Chan, M. N., Huang, D. D.,
949 and Ge, X.: Co-photolysis of mixed chromophores affects atmospheric lifetimes of brown carbon,
950 Environmental Science: Atmospheres, 3, 1145-1158, 2023b.

951 Wang, Y., Zhang, Q., Jiang, J., Zhou, W., Wang, B., He, K., Duan, F., Zhang, Q., Philip, S., and Xie, Y.:
952 Enhanced sulfate formation during China's severe winter haze episode in January 2013 missing from
953 current models, Journal of Geophysical Research: Atmospheres, 119, 10,425-410,440,
954 <https://doi.org/10.1002/2013JD021426>, 2014.

955 Wang, Y., Hu, M., Lin, P., Guo, Q., Wu, Z., Li, M., Zeng, L., Song, Y., Zeng, L., Wu, Y., Guo, S., Huang,
956 X., and He, L.: Molecular Characterization of Nitrogen-Containing Organic Compounds in Humic-like
957 Substances Emitted from Straw Residue Burning, Environmental Science & Technology, 51, 5951-5961,
958 10.1021/acs.est.7b00248, 2017b.

959 Woods, E., III, Harris, O. T., Leiter, W. E., Burner, N. E., Ofosuhene, P., Krez, A., Hilton, M. A., and
960 Burke, K. A.: Lifetime of Triplet Photosensitizers in Aerosol Using Time-Resolved Photoelectric Activity,
961 ACS Earth and Space Chemistry, 4, 1424-1434, 10.1021/acsearthspacechem.0c00141, 2020.

962 Wu, C.-H., Yuan, C.-S., Yen, P.-H., Yeh, M.-J., and Soong, K.-Y.: Diurnal and seasonal variation,
963 chemical characteristics, and source identification of marine fine particles at two remote islands in South
964 China Sea: A superimposition effect of local emissions and long-range transport, Atmospheric
965 Environment, 270, 118889, <https://doi.org/10.1016/j.atmosenv.2021.118889>, 2022.

966 Wyant, M. C., Bretherton, C. S., Wood, R., Carmichael, G. R., Clarke, A., Fast, J., George, R., Gustafson
967 Jr, W. I., Hannay, C., Lauer, A., Lin, Y., Morcrette, J. J., Mulcahy, J., Saide, P. E., Spak, S. N., and Yang,
968 Q.: Global and regional modeling of clouds and aerosols in the marine boundary layer during VOCALS:
969 the VOCA intercomparison, Atmos. Chem. Phys., 15, 153-172, 10.5194/acp-15-153-2015, 2015.

970 Xie, M., Chen, X., Hays, M. D., and Holder, A. L.: Composition and light absorption of N-containing

971 aromatic compounds in organic aerosols from laboratory biomass burning, *Atmos. Chem. Phys.*, 19,
972 2899-2915, 10.5194/acp-19-2899-2019, 2019.

973 Yan, X., Bain, R. M., and Cooks, R. G.: Organic Reactions in Microdroplets: Reaction Acceleration
974 Revealed by Mass Spectrometry, *Angewandte Chemie International Edition*, 55, 12960-12972,
975 <https://doi.org/10.1002/anie.201602270>, 2016.

976 Yang, M., Zhang, H., Chang, F., and Hu, X.: Self-sensitized photochlorination of benzo[a]pyrene in saline
977 water under simulated solar light irradiation, *Journal of Hazardous Materials*, 408, 124445,
978 <https://doi.org/10.1016/j.jhazmat.2020.124445>, 2021.

979 Yao, M., Zhao, Y., Hu, M., Huang, D., Wang, Y., Yu, J. Z., and Yan, N.: Multiphase reactions between
980 secondary organic aerosol and sulfur dioxide: kinetics and contributions to sulfate formation and aerosol
981 aging, *Environmental Science & Technology Letters*, 6, 768-774, 2019.

982 Ye, C., Lu, K., Song, H., Mu, Y., Chen, J., and Zhang, Y.: A critical review of sulfate aerosol formation
983 mechanisms during winter polluted periods, *Journal of Environmental Sciences*, 123, 387-399,
984 <https://doi.org/10.1016/j.jes.2022.07.011>, 2023.

985 Ye, J., Abbatt, J. P., and Chan, A. W.: Novel pathway of SO₂ oxidation in the atmosphere: reactions with
986 monoterpene ozonolysis intermediates and secondary organic aerosol, *Atmospheric Chemistry and
987 Physics*, 18, 5549-5565, 2018.

988 Zhang, L., Hu, B., Liu, X., Luo, Z., Xing, R., Li, Y., Xiong, R., Li, G., Cheng, H., Lu, Q., Shen, G., and
989 Tao, S.: Variabilities in Primary N-Containing Aromatic Compound Emissions from Residential Solid
990 Fuel Combustion and Implications for Source Tracers, *Environmental Science & Technology*, 56, 13622-
991 13633, 10.1021/acs.est.2c03000, 2022.

992 Zhang, R. and Chan, C. K.: Simultaneous formation of sulfate and nitrate via co-uptake of SO₂ and NO
993 2 by aqueous NaCl droplets: combined effect of nitrate photolysis and chlorine chemistry, *Atmospheric
994 Chemistry and Physics*, 23, 6113-6126, 2023a.

995 Zhang, R. and Chan, C. K.: Simultaneous formation of sulfate and nitrate via co-uptake of SO₂ and NO₂
996 by aqueous NaCl droplets: combined effect of nitrate photolysis and chlorine chemistry, *Atmos. Chem.
997 Phys.*, 23, 6113-6126, 10.5194/acp-23-6113-2023, 2023b.

998 Zhang, R. and Chan, C. K.: Enhanced Sulfate Formation through Synergistic Effects of Chlorine
999 Chemistry and Photosensitization in Atmospheric Particles, *ACS ES&T Air*, 1, 92-102,
1000 10.1021/acsestair.3c00030, 2024.

1001 Zhang, R., Gen, M., Huang, D., Li, Y., and Chan, C. K.: Enhanced Sulfate Production by Nitrate
1002 Photolysis in the Presence of Halide Ions in Atmospheric Particles, *Environmental Science & Technology*,
1003 54, 3831-3839, 10.1021/acs.est.9b06445, 2020a.

1004 Zhang, S., Li, D., Ge, S., Wu, C., Xu, X., Liu, X., Li, R., Zhang, F., and Wang, G.: Elucidating the
1005 Mechanism on the Transition-Metal Ion-Synergetic-Catalyzed Oxidation of SO₂ with Implications for
1006 Sulfate Formation in Beijing Haze, *Environmental Science & Technology*, 58, 2912-2921,
1007 10.1021/acs.est.3c08411, 2024.

1008 Zhang, S., Li, D., Ge, S., Liu, S., Wu, C., Wang, Y., Chen, Y., Lv, S., Wang, F., Meng, J., and Wang, G.:
1009 Rapid sulfate formation from synergetic oxidation of SO₂ by O₃ and NO₂ under ammonia-rich
1010 conditions: Implications for the explosive growth of atmospheric PM_{2.5} during haze events in China,
1011 *Science of The Total Environment*, 772, 144897, <https://doi.org/10.1016/j.scitotenv.2020.144897>, 2021a.

1012 Zhang, T., Dong, J., Zhang, C., Kong, D., Ji, Y., Zhou, Q., and Lu, J.: Photo-transformation of
1013 acetaminophen sensitized by fluoroquinolones in the presence of bromide, *Chemosphere*, 327, 138525,
1014 <https://doi.org/10.1016/j.chemosphere.2023.138525>, 2023.

1015 Zhang, Y., Wang, K., Tong, H., Huang, R.-J., and Hoffmann, T.: The maximum carbonyl ratio (MCR) as
1016 a new index for the structural classification of secondary organic aerosol components, *Rapid*
1017 *Communications in Mass Spectrometry*, 35, e9113, <https://doi.org/10.1002/rcm.9113>, 2021b.

1018 Zhang, Y., Bao, F., Li, M., Xia, H., Huang, D., Chen, C., and Zhao, J.: Photoinduced Uptake and
1019 Oxidation of SO₂ on Beijing Urban PM_{2.5}, *Environmental Science & Technology*, 54, 14868-14876,
1020 10.1021/acs.est.0c01532, 2020b.

1021 Zhao, R., Zhang, Q., Xu, X., Wang, W., Zhao, W., Zhang, W., and Zhang, Y.: Effect of photooxidation
1022 on size distribution, light absorption, and molecular compositions of smoke particles from rice straw
1023 combustion, *Environmental Pollution*, 311, 119950, <https://doi.org/10.1016/j.envpol.2022.119950>, 2022.

1024 Zherebker, A., Rukhovich, G. D., Sarycheva, A., Lechtenfeld, O. J., and Nikolaev, E. N.: Aromaticity
1025 Index with Improved Estimation of Carboxyl Group Contribution for Biogeochemical Studies,
1026 *Environmental Science & Technology*, 56, 2729-2737, 10.1021/acs.est.1c04575, 2022.

1027 Zhong, S., Liu, R., Yue, S., Wang, P., Zhang, Q., Ma, C., Deng, J., Qi, Y., Zhu, J., and Liu, C.-Q.: Peatland
1028 Wildfires Enhance Nitrogen-Containing Organic Compounds in Marine Aerosols over the Western
1029 Pacific, *Environmental Science & Technology*, 2024.

1030 Zhou, L., Liang, Z., Mabato, B. R. G., Cuevas, R. A. I., Tang, R., Li, M., Cheng, C., and Chan, C. K.:
1031 Sulfate formation via aerosol-phase SO₂ oxidation by model biomass burning photosensitizers: 3,4-
1032 dimethoxybenzaldehyde, vanillin and syringaldehyde using single-particle mixing-state analysis, *Atmos.*
1033 *Chem. Phys.*, 23, 5251-5261, 10.5194/acp-23-5251-2023, 2023.

1034